NASA Contractor Report 195303

Analysis of New Composite Architectures

John D. Whitcomb
Texas A&M University
College Station, Texas 77843–3141

April 1994

Prepared for
Lewis Research Center
Under Grant NAG3–1270

National Aeronautics and
Space Administration

ANAYLSIS OF NEW COMPOSITE ARCHITECTURES

NASA Grant NAG3-1270

Interim Report

July 1, 1992 - June 30, 1993

submitted by

John D. Whitcomb
Aerospace Engineering Department
and

CENTER for MECHANICS of COMPOSITES
Texas A&M University
College Station, Texas 77843-3141

to .

NASA Lewis Research Center
Cleveland, Ohio 44135

October 1993

Analysis of New Composite Architectures

John Whitcomb
Aerospace Engineering Department and
Center for Mechanics of Composites
Texas A&M University
College Station TX 77843-3141

Review of Second Year

This document describes progress during the second year of the NASA Grant NAG3-1270. Funding for this grant began May 1, 1991. This report covers the period July 1, 1992 to June 30, 1993.

This grant has helped support three students who graduated in this grant year. Sitaram Gundapaneni graduated in December 1992 with a master's degree. Kyeongsik Woo graduated in August 1993 with a PhD degree. Gopal Kondagunta graduated in August 1993 with a master's degree. The last two actually finished all their work in late spring of 1993. Copies of the theses have already been sent to the technical monitor, so they will not be included in this document. Presentations were made at two national conferences and one workshop. A paper titled "Enhanced Direct Stiffness Method for Finite Element Analysis of Textile Composites" was presented at the 1992 ASME winter annual meeting in November 1992. A paper titled "Global/Local Finite Element Analysis for Textile Composites" was presented at the 33rd SDM conference in April 1993. A paper titled "Boundary Effects in Textile Composites" was presented at a workshop sponsored by NASA Langley Research Center in July, 1993. This paper was also presented at the Second U.S. National Congress on Computational Mechanics in August 1993. A copy of the first paper was included in last year's report. Copies of papers related to the other two talks have been included in this report. Details of the research can be found in the papers and theses. While we are encouraged by the results to date, our studies indicate that the current technique for interfacing of global and local models is not as accurate as we had hoped. The current technique involves exact displacement constraints. Because of the crudeness of the global model, this interfacing technique results in significant artifacts in the stress distributions near the global/local boundary. Of course, one could just include a larger region in the local model if there are sufficient computer resources. A high priority this year will be improving the global/local interfacing by using variations of mixed boundary constraints. This will result in some local violation of compatibility, but it might reduce the artifacts near the boundary. A variety of computer programs have been developed with the help of this grant. The primary programs will be documented during the third year and submitted to COSMIC.

GLOBAL/LOCAL FINITE ELEMENT ANALYSIS FOR TEXTILE COMPOSITES

by

Kyeongsik Woo
John Whitcomb
Department of Aerospace Engineering
Texas A&M University
College Station, Texas, 77843-3141

Abstract

Conventional finite element analysis of textile composites is impractical because of the complex microstructure. Global/local methodology combined with special macro elements is proposed herein as a practical alternative. Initial tests showed dramatic reductions in the computational effort with only a small loss in accuracy.

Introduction

There is a growing interest in the use of textile architectures for advanced composite structures. Textile materials are known to have improved interlaminar properties and impact resistance. Due to the complicated architecture, analysis of textile structures is very challenging. One of the difficulties is the wide range of structural scales which must be considered.

Figure 1 illustrates the microstructural scales. The basic repeating microstructural element in this figure is labeled 'coarse microstructure'. At this level, the very distinctive phases of textile composites are observed and discrete material modelling is needed. In contrast, there could be a level where a very large number of unit cells are considered. At this level, the characteristic dimensions are of the order of the structural elements, and the material appears almost homogeneous (schematic labeled as 'fine microstructure') and homogenized engineering properties can be used. In between these two levels lies another level of microstructure: the transitional level. At this level, there are too many microstructural details to model each discretely. Furthermore, the microstructural scale is too large to use homogenized engineering properties.

Because of the different levels of microstructure, global/local finite element method can be one of the more efficient analysis methods for textile composite structures. Global/local finite element analysis is often used to study the stress distribution in a small portion of structures in great detail [1-5]. In this method, a relatively crude global mesh is used to obtain the overall response of the structure and refined local meshes are used in the regions of interest where rapid stress changes may occur. In analyzing a textile composite structure by the global/local method, a relatively crude global mesh with homogenized material properties can be used at the fine microstructural level. In the local meshes, the details of the coarse microstructure of textile

composites (eg. the individual tows and matrix pockets) are modelled discretely. However, in the transitional range of microstructure, discrete modelling is not practical even with supercomputers due to the huge computer memory and cpu requirements. Use of homogenized material properties is also often inappropriate. In this range, special finite elements are needed which can account for microstructure within a single element.

References [6-8] discuss some possibilities. The elements described in these references are based on single or multiple assumed displacement fields. These elements are referred to by the authors as single-field [6,7] and multi-field [8] macro elements, respectively. Due to the multiple assumed displacement fields, the multi-field macro elements produce much more accurate results than the single-field macro elements. However, the multi-field macro elements are more costly to use than the single-field macro elements. Herein, single-field macro elements were used. However, the basic procedure is the same whether single-field or multi-field macro elements are used.

In this paper, the global/local finite element method is used for stress analysis of plain weave textile composites. Single-field macro elements were used for the global mesh and conventional finite elements were used for the local mesh. The effectiveness of the proposed global/local procedure was studied in terms of the accuracy of the calculated local stresses. The effect of using the iterative or non-iterative global/local procedures on accuracy was also discussed.

Analysis

This section briefly describes the theory for global/local analysis and macro elements. More details can be found in references [5] and [6].

Iterative Global/Local Method

The total global solution can often be obtained by solving several subproblems. These subproblems are solved separately, while the interaction across the subregion boundaries is handled by iterative solution. These ideas are particularly attractive if several substructures are identical or if some of them have been analyzed previously [9]. In fact, in the preliminary design stage, a large number of analyses are performed with small local design change. Such is also the case when solving damage growth problems.

Figure 2 shows a schematic of the iterative global/local method used. Initially the global problem is solved. Traditional finite elements with smeared engineering properties, single-field macro elements, or multi-field macro elements are used in the global mesh. After obtaining the global response, the global/local boundary displacements are applied to a local mesh as a boundary condition and the local problem is solved. Due to the difference in mesh refinement in the local region, there is a violation in equilibrium at the global/local boundary. This force unbalance is defined by

$$\Psi_\alpha = \int_A \sigma_{ij} \frac{\partial \epsilon_{ij}}{\partial q_\alpha} dV + \int_C \sigma_{ij} \frac{\partial \epsilon_{ij}}{\partial q_\alpha} dV - F_\alpha \qquad (1)$$

where F_α is the externally applied nodal force vector and q_α are the nodal displacements. Global/local iteration can be used to eliminate the residuals. Iteration is repeated until sufficiently small residuals are obtained.

Note that the regions which need further refinement are not known *a priori* in general. Therefore, a standard procedure for the global/local method with local refinement would be

(1) perform global analysis
(2) find local regions of interest
(3) define refined meshes for the local regions
(4) perform global/local iterations

The initial coarse global mesh can serve as the global mesh for the global/local iterations. If a direct solver is used, the decomposed global stiffness matrix is already available at this point. Since the initial global solution is required to identify the regions of interest, the cost for the global/local iterations is relatively cheap.

This global/local method with local refinement assumes that the region which requires further mesh refinement can be localized. If the solution behavior is complicated everywhere, the correction by the global/local iteration does not necessarily reflect the nature of the true solution accurately. For example, if the solution behavior is complicated everywhere and only some portion of the global domain is refined in the local mesh, the global/local iteration may do more harm than good in solving the problem. This possibility was tested in this study and turned out to be so. A solution to this problem is using an engineering global/local analysis. In this procedure, the initial coarse global solution is assumed to be close enough for the purpose at hand. That is, no global/local iteration is employed. The local problem is solved only once with boundary displacements from the coarse global solution. This procedure is often used in engineering practices and serves well for the approximate solution at the initial design stage. In this paper, the local mesh nodal displacements at the global/local boundary were obtained by interpolation using the finite element shape functions for the coarse global mesh.

Macro Finite Elements

In the following, the formulation of single-field macro elements using subdomain integration is described.

Figure 3 shows a typical finite element mesh used to define a four-node macro element. The symbol q denotes the nodal displacement vector. Subscripts m, i, and b represent *macro*, *internal* and *boundary* nodal degrees of freedom (dof), respectively. The stiffness matrix and force vector for this mesh is

$$\begin{bmatrix} K_{ii} & K_{ib} \\ K_{bi} & K_{bb} \end{bmatrix} \begin{bmatrix} q_i \\ q_b \end{bmatrix} = \begin{bmatrix} f_i \\ f_b \end{bmatrix} \qquad (2)$$

To obtain the macro element stiffness matrix, all the dof except the macro element dof are eliminated or slaved. In single-field macro elements, multi-point constraints are used to slave the internal and excess boundary dof. In multi-field macro elements, static condensation is used to condense out internal dof and multi-point constraints are used to slave the excess boundary dof. For single-field macro elements, the macro element stiffness matrix can be expressed as

$$[K_m] = [T]^T[K][T] \tag{3}$$

where

$$\{q\} = [T]\{q_m\} \tag{4}$$

and for multi-field macro elements, this can be expressed as

$$[K_m] = [T]^T[\bar{K}_{bb}][T] \tag{5}$$

where

$$\{q_b\} = [T]\{q_m\} \tag{6}$$

$$[\bar{K}_{bb}] = [K_{bb}] - [K_{bi}][K_{ii}]^{-1}[K_{ib}] \tag{7}$$

The single-field macro element used in this paper is described in reference *6*. Rather than explicitly using a transformation matrix, this single-field macro element divides the integration domain into subdomains and uses three coordinate systems to facilitate the numerical integration. Figure 4 illustrates schematically the mapping procedure between the coordinate systems. As seen in the figure, the contribution of the p-th subdomain to the macro element stiffness matrix can be written as

$$[K]_p = \int_{-1}^{1}\int_{-1}^{1}[B]^T[D]_p[B]\,|J_1|\,|J_2|\,dr\,ds \tag{8}$$

where

$$J_1 = \frac{\partial(x,y)}{\partial(\xi,\eta)}, \quad J_2 = \frac{\partial(\xi,\eta)}{\partial(r,s)} \tag{9}$$

The single-field macro element stiffness is then given by

$$[K_m] = \sum_{p=1}^{n} [K]_p \tag{10}$$

Note that only one set of functions is used for the displacement interpolation.

Configuration

Figure 5 shows a conventional two dimensional finite element mesh for a plain weave textile composite. The figure shows a symmetrically stacked textile structure with six plain weave mats. The plain weave textile mat was described by two parameters: the wavelength of the fiber bundle "*a*" and the thickness of the textile mat "*b*". The waviness of plain weave textile composites was defined to be

$$Waviness = b/a$$

In this study, the waviness of the plain weave mat was 0.333.

The basic repeating unit cells are easily distinguished and nine complete unit cells are present. Each unit cell is composed of three material groups; 0° tows, 90° tows, and pure resin pockets. The material properties of the fiber bundles and resin pockets were assumed to be [10]

Fiber bundles (Graphite/Epoxy):

$$E_{11} = 206.9 \text{ GPa}, E_{22} = E_{33} = 5.171 \text{ GPa}$$
$$\nu_{12} = \nu_{13} = \nu_{23} = 0.25$$
$$G_{12} = G_{13} = G_{23} = 2.386 \text{ GPa}$$
$$X_t = 1034. \text{ MPa}, Y_t = Z_t = 41.37 \text{ MPa}$$
$$X_c = 689.5 \text{ MPa}, Y_c = Z_c = 117.2 \text{ MPa}$$
$$S_{12} = S_{23} = S_{13} = 68.96 \text{ MPa}$$

Resin (Epoxy):

$$E = 3.45 \text{ GPa}, \nu = 0.35, G = 1.28 \text{ GPa}$$
$$X_t = 103.4 \text{ MPa}, X_c = 241.3 \text{ MPa}, S = 89.6 \text{ MPa}$$

Plane strain conditions were imposed to obtain the two dimensional constitutive properties.

Figure 6 shows a global/local mesh. The textile structure in figure 5 is discretized coarsely first using macro elements (region $A+B$), and then one of the unit cells (region B) is refined (region C) for detailed analysis. Four-node, eight-node, or twelve-node single-field macro elements were used for the global mesh. Four-node conventional finite elements were used for the refined local mesh. The degree of refinement of the local mesh was the same as the conventional mesh shown in figure 5. Since the geometry of plain weave textile composites has a distinct repeating pattern, only two types of macro elements were needed. Once the stiffness matrices for those two types of macro elements were obtained, these stiffness matrices were reused for the rest of the global elements.

Table 1 shows the number of nodes, number of elements, and computer storage requirements for the classical and global/local finite element meshes. The table indicates that the saving in computer memory was huge. For more complicated or larger problems, this saving is expected to be greater.

Table 1. List of number of nodes, number of elements, and profile storage requirements.

		NN	NE	Profile
Global:	12-node	217	36	19131
	8-node	133	36	7911
	4-node	49	36	1499
Local:	4-node	886	864	99083
Conventional:	4-node	7645	7776	2065827

Results and Discussion

This section discusses numerical results for the global/local analysis of two dimensional plain weave textile composites. The two dimensional nine unit cell model of plain weave textile composite was loaded uniaxially in the x-direction. The top and bottom surfaces were traction free. The applied nominal strain was 0.005.

Figure 7 shows the global/local iteration history in terms of maximum residuals at the global/local boundary versus iteration number. Four-node, eight-node, and twelve-node macro elements were used for the global mesh. The figure shows fast convergence for all cases. Note that for higher order elements, the initial maximum residual was smaller since better global/local boundary displacement interpolation was obtained with higher order shape functions while the convergence was slower since more degrees of freedom were involved in the global/local iterations.

Figure 8 shows the σ_{11} stress contours by the conventional FEM, the iterative global/local analysis, and the non-iterative engineering global/local analysis. Twelve-node macro elements were used for the global mesh. For the local mesh and the conventional mesh, four-node elements were used. The stress contours were for the upper left fiber bundle of the center unit cell indicated in the figure. The stress was transformed to the material axes. Surprisingly, the results by the non-iterative global/local analysis were better than those from the iterative global/local analysis. Figure 9 shows the σ_{11} stress distribution of the fiber bundle along the fiber bundle boundary FB6 indicated in the figure. This figure also shows an excellent agreement in the stress distribution by the conventional FEM and the non-iterative global/local method. The iterative global/local analysis predicted much higher stress compared to the conventional finite element analysis result.

The global/local iteration was employed to eliminate the force residual at the global/local boundary. The force residual at the global/local boundary was due to the difference in the mesh refinement of the local region (shaded region in Figure 9) between the global and local meshes. For the local region, the stiffness matrix with the coarse global mesh was stiffer, while it was softer with the refined local mesh. Thus, for the iterative global/local analysis it is as though the shaded local region was replaced by a softer material. The softer region resulted in larger displacements and thus resulted in higher predicted stresses.

The fiber bundle stress distributions were plotted along the 0° fiber bundle boundaries. Figure 10 defines the fiber bundle boundaries FB2, FB3, Fb4, and Fb6 for the stress plotting. Figure 11 shows the σ_{11} distribution of the fiber bundles along the fiber bundle boundaries FB2 and FB4. The stress was calculated by the conventional FEM (C) and by the global/local analysis with four-node (M1), eight-node (M2), and twelve-node (M3) macro elements. Since the non-iterative global/local analysis was found to be better in predicting the stress distribution for the current textile composite configuration, the stress was obtained using the non-iterative global/local analysis. Figure 11(a) shows that along FB2 the stress obtained by the global/local analysis was agreed well with that by the conventional FEM. Even the global/local analysis with the four-node macro elements performed very well except the regions near the global/local boundary (*ie.* close to x/b=+1.5, -1.5).

Figure 11(b) shows the stress distribution along FB4. Note that the FB4 path is much closer to the global/local boundary than FB2. The stress results by the global/local analysis with eight-node and twelve-node macro elements were acceptable away from the global/local boundary. However, the agreement was poor near the global/local boundary regions (*ie.* x/b=+1.5, 0, -1.5).

The disagreement near the global/local boundary regions was due to the low order displacement interpolation from the global solution. For better solutions, one can use higher order macro elements (*p*-refinement) or smaller macro elements (*h*-refinement) for the global mesh. Both will improve the global response as well as the global/local boundary displacement communication. However, even for the coarse global mesh with low order macro elements the disagreement near the boundary regions is not a prohibitive concern since the definition of local regions is quite arbitrary. If one finds a region of interest, one can simply define the corresponding local mesh in such a way that the region of interest is located at the center of the local mesh. Away from the global/local boundary, the stress results from the non-iterative engineering global/local analysis was found to be quite accurate.

Figure 12 shows σ_{11} and σ_{33} distributions along FB2, FB3, and FB6. The stresses were calculated by the global/local method with twelve-node macro elements. The stress distributions

along these fiber bundle boundaries would be exactly the same if there was no free surface effect. However, this figure shows that the stress distributions along FB2, which was close to the free boundary, were different from those along FB3 and FB6, which were further inside. The difference between the stress distributions along FB3 and FB6 was very small. The free surface effects can be seen very graphically in Figure 13, which shows σ_{11} and σ_{33} stress contours for the upper three mats. The stresses were transformed to the material axes and normalized by the strengths. This figure shows that the stress distribution in layers 2 and 3 are almost mirror images, which indicates that the free surface does not significantly affect either layer. The stress distribution in layer 1 is much different from that in layers 2 and 3 because of the free surface effect. From these figures, one can conclude that the free surface effect plays an important role on the stress distribution in the surface layers of textile structures. For thick textile structures, the contribution of the boundary effect may be negligible. However, even for thick textile structures, the free surface effect should be considered in failure analysis, since the failure can initiate near the free boundary.

Conclusion

A two dimensional plain weave textile structure was analyzed using the conventional and global/local finite element methods. In the global/local analysis, single-field macro elements using subdomain integration were used for the global mesh. For the local mesh in the global/local analysis and for the classical finite element mesh, the fiber tow geometry was modeled discretely.

In this study, the global/local procedure with macro elements was found to be very efficient for the detailed stress analysis for textile composites. The complicated geometry makes discrete modeling impractical for realistic three dimensional analysis because of huge computer memory and cpu time. With the use of macro elements, global/local finite element analysis permits the detailed analysis for textile composite structures.

It is shown that the iterative global/local method was not the best choice for textile composites. In this study, the non-iterative engineering global/local method predicted the local stress better than the iterative global/local method. The stress results from the non-iterative global/local analysis were acceptable except near the global/local boundary. More study is needed to improve stress calculation near the global/local boundary.

The stress distribution near the free boundary of the plain weave textile composites was found to be different from that inside. Thus, for the detailed stress and failure analysis, the free boundary effect must be considered.

Acknowledgement

This work was supported by NASA Lewis Research Center Grant NAG3-1270 and by NASA Langley Research Center Grant NAG1-1324. The technical monitors are Dr. C.C. Chamis and J.R. Reeder, respectively. This support is gratefully acknowledged.

References

1. Hirai, I., Uchiyama, T., Mizuta, Y., and Pilkey, W., An Exact Zooming Method, Finite Elements in Analysis and Design 1, Elsevier Science Publishers, pp. 61-69, 1985.
2. Jara-Alamonte, C. and Knight, C., The Specified Boundary Stiffness/Force SBSF Method for Finite Element Subregion Analysis, International Journal for Numerical Methods in Engineering, Vol. 26, pp. 1567-1578, 1988.
3. Whitcomb, J.D., Iterative Global/Local Finite Element Analysis, Computers & Structures, Vol. 40, No.4, 1991.
4. Fish, J. and Markolefas, S., The s-Version of The Finite Element Method for Multilayer Laminates, International Journal for Numerical Methods in Engineering, Vol. 33, pp. 1081-1105, 1992.
5. Whitcomb, J.D. and Woo, K., Application of Iterative Global/Local Finite Element Analysis, Part II: Geometrically Nonlinear Analysis, To be published in Communications of Numerical Methods in Engineering.
6. Woo, K. and Whitcomb, J.D., Macro Finite Element Using Subdomain Integration, To be published in Communications of Numerical Methods in Engineering.
7. Whitcomb, J.D., Woo., K., and Gundapaneni, S., Macro Finite Element for Analysis of Textile Composites, Proceeding of the 6th Japan-U.S. Conference on Composite Materials, Orlando FL, June 22-24, 1992.
8. Whitcomb, J.D., Woo., K., Enhanced Direct Stiffness Method for Finite Element Analysis of Textile Composites, Proceedings of 1992 ASME Winter Annual Meeting, Anaheim CA, November 8-13, 1992.
9. Bjorstad, P.E. and Widlund, O.B., Iterative Methods for the Solutions of Elliptic Problems on Regions Partitioned Into Substructures, SIAM Journal on Numerical Analysis, Vol. 23, No. 6, December 1986.
10. Jones, R.M., Mechanics of Composite Materials, Scripta Book Company, Washingon D.C., 1975.

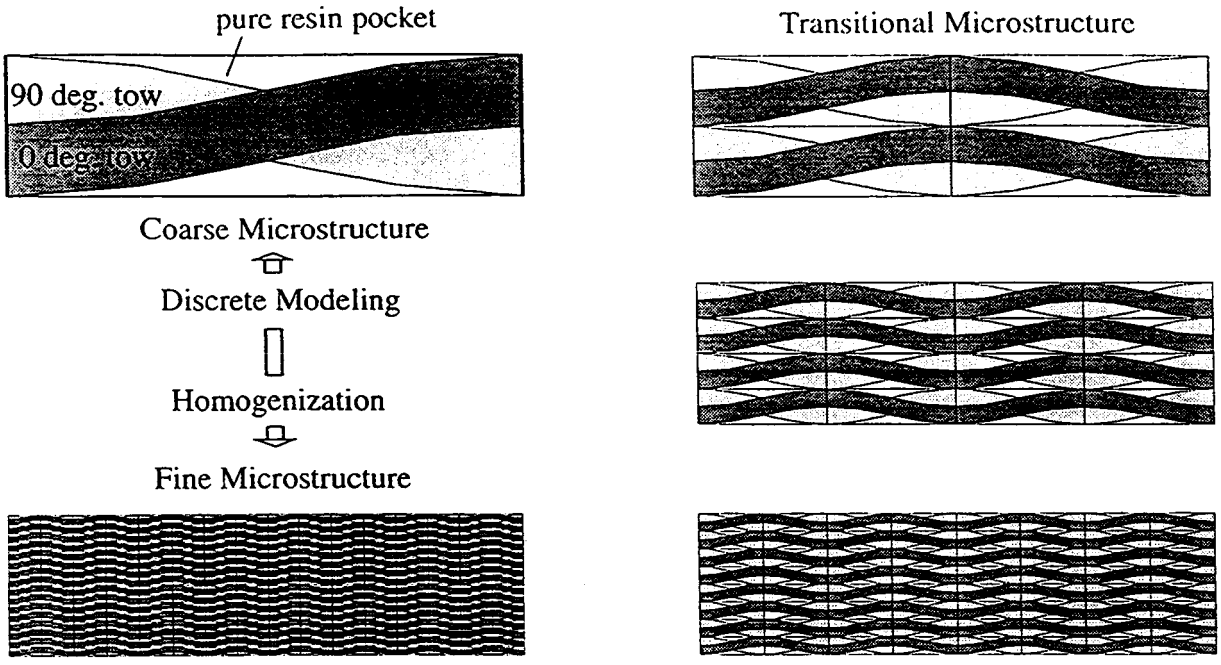

Fig.1. Microstructural scales of textile composites.

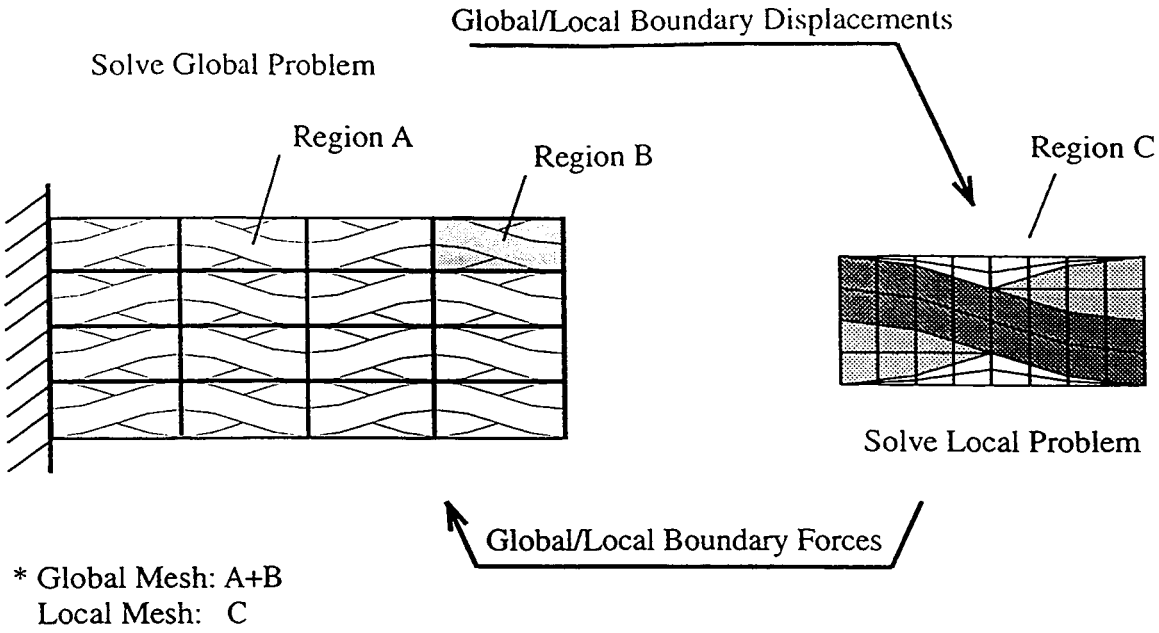

Fig.2. Schematic of iterative global/local analysis.

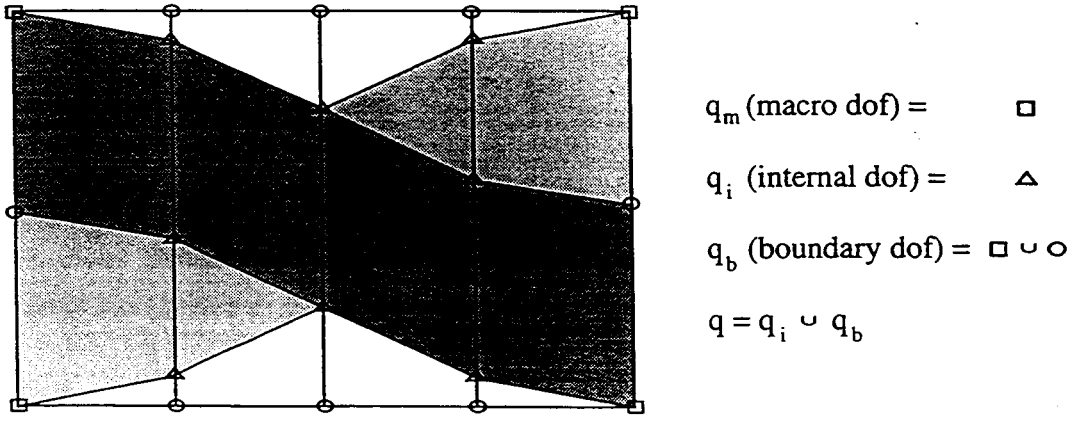

Fig.3. A typical submesh for a macro element.

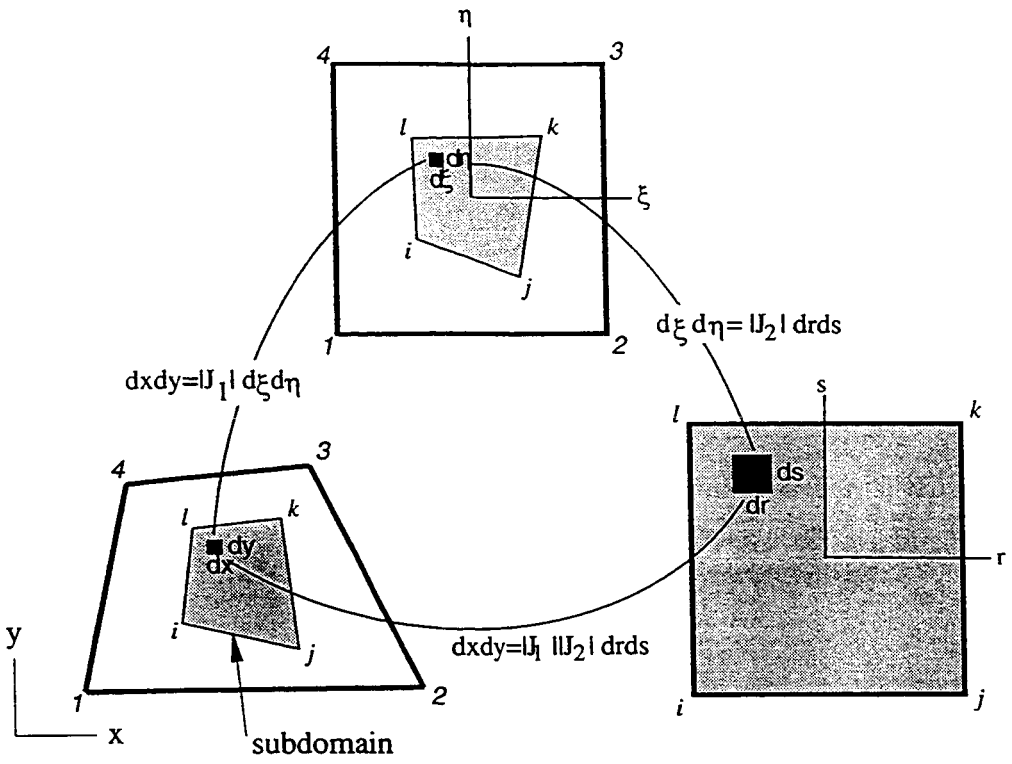

Fig.4. Mapping in three coordinate systems.

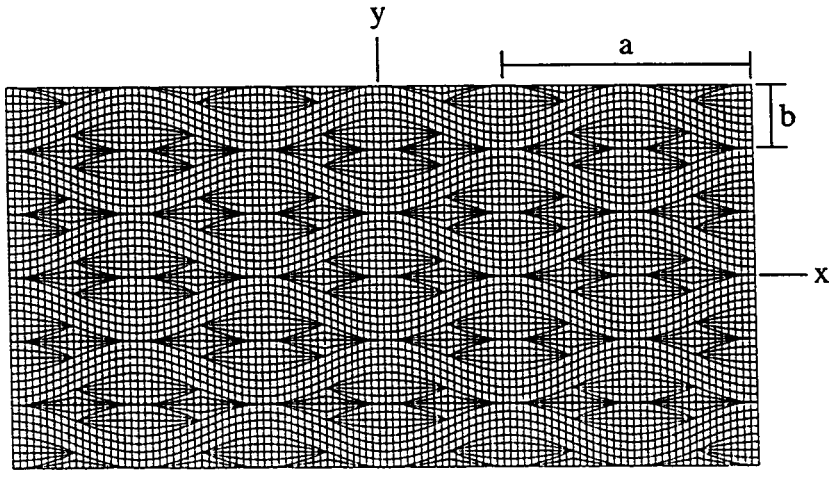

Fig.5. A conventional finite element mesh for a six symmetrically stacked plane weave textile mats. (Number of nodal points = 7645, Number of elements = 7776)

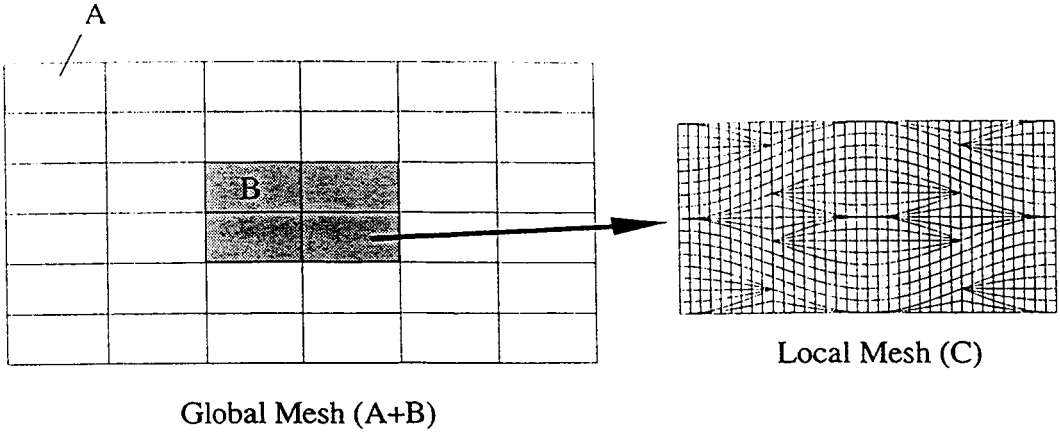

Fig.6. Coarse global mesh and refined local mesh.

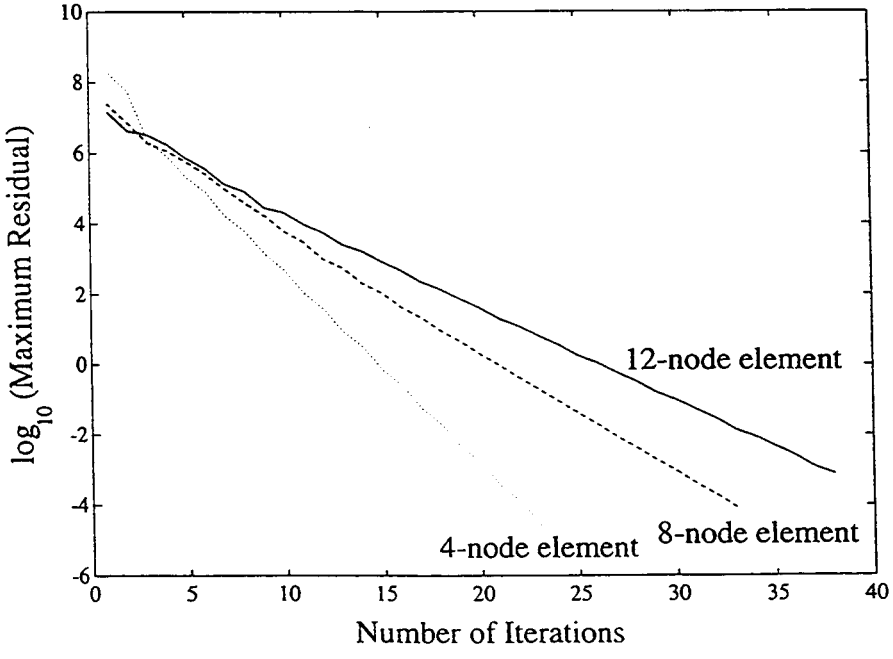

Fig.7. Maximum residual versus iteration number for plain weave textile composite under uniaxial tension in x-direction. Three different global macro elements were used: 4-node, 8-node, and 12-node single-field macro elements.

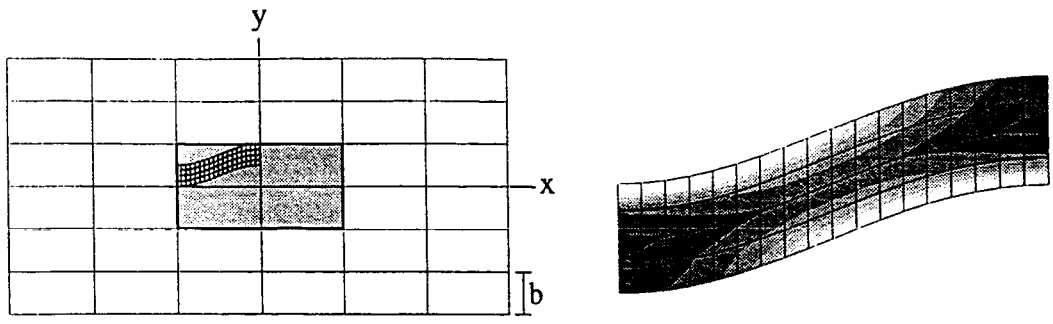

(a) Conventional FEM

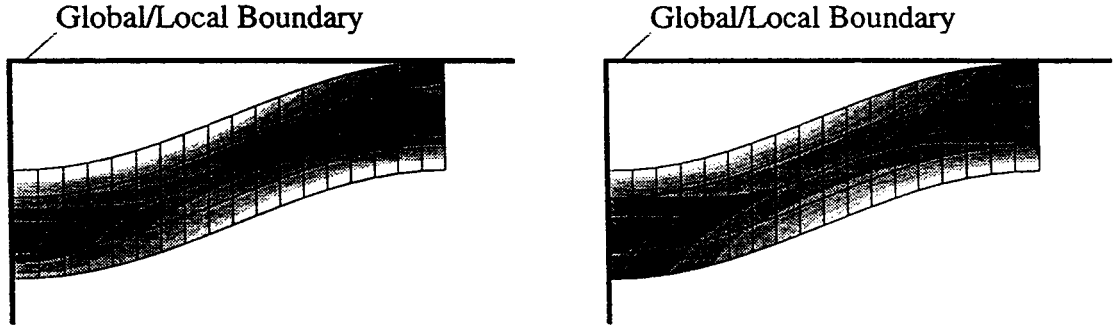

(b) Iterative global/local method

(c) Engineering global/local method

Fig.8. Contour plots of σ_{11} by conventional FEM, iterative global/local method, and engineering global/local method. The stress contours were for the upper left fiber bundle of the center unit cell.

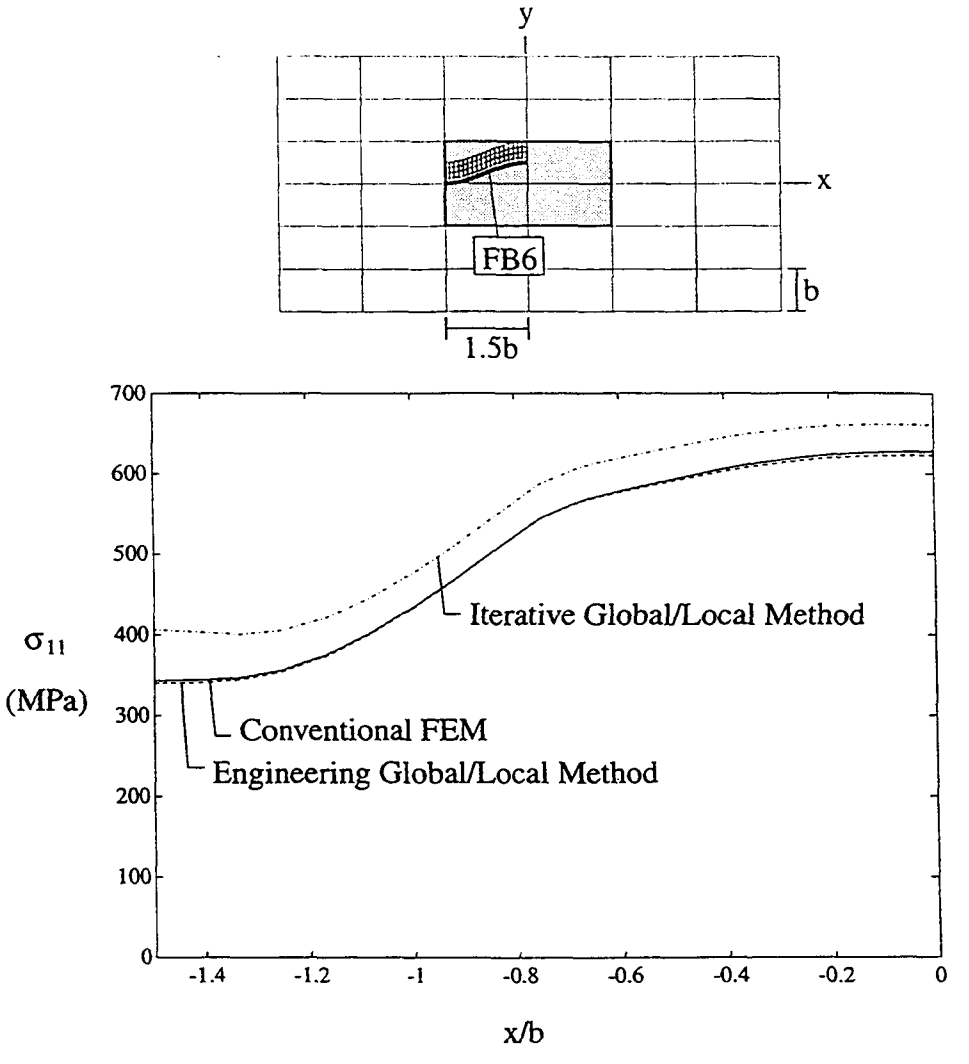

Fig.9. Distribution of σ_{11} by conventional FEM, iterative global/local method, and engineering global/local method. The stress distribution was along the fiber bundle boundary FB6 indicated in the figure.

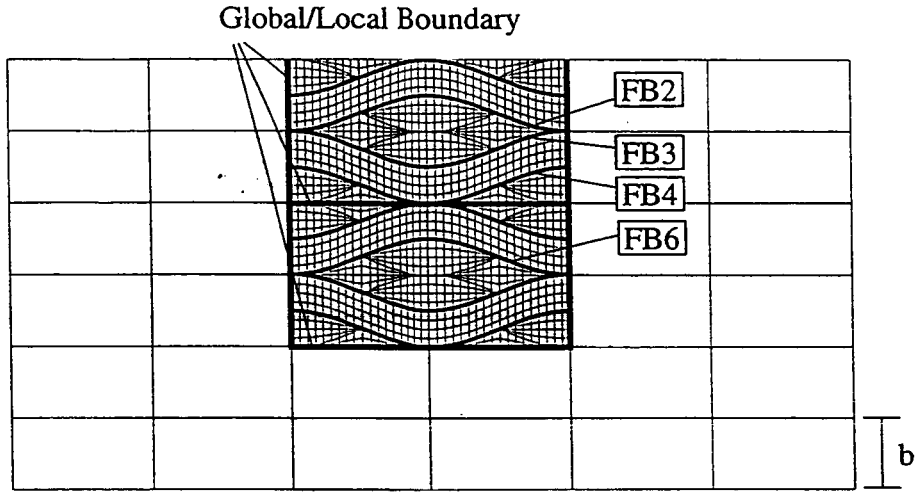

Fig.10. Definition of paths for stress plotting.

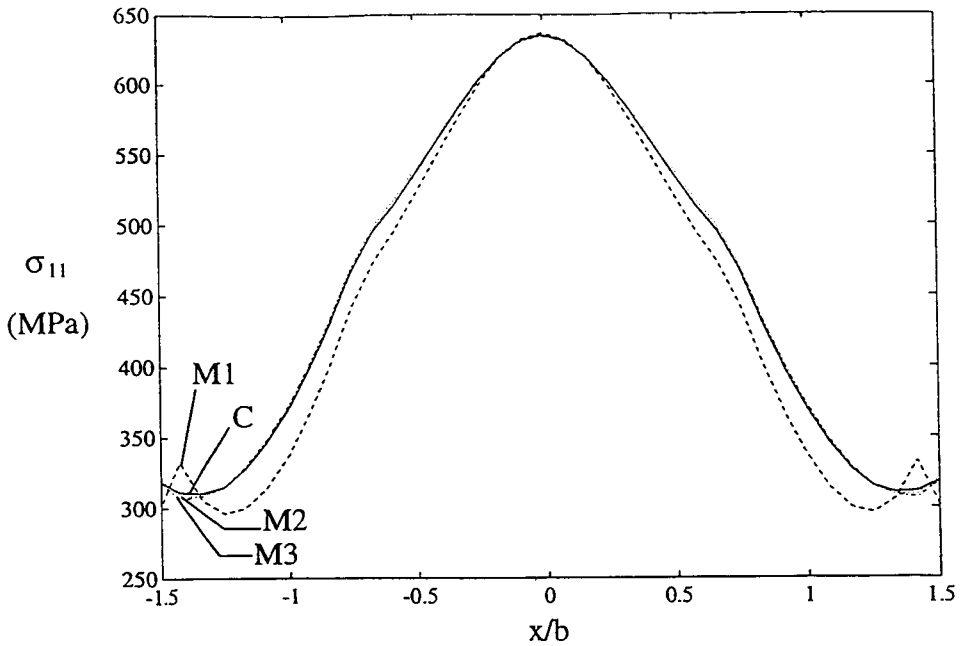

(a) FB2

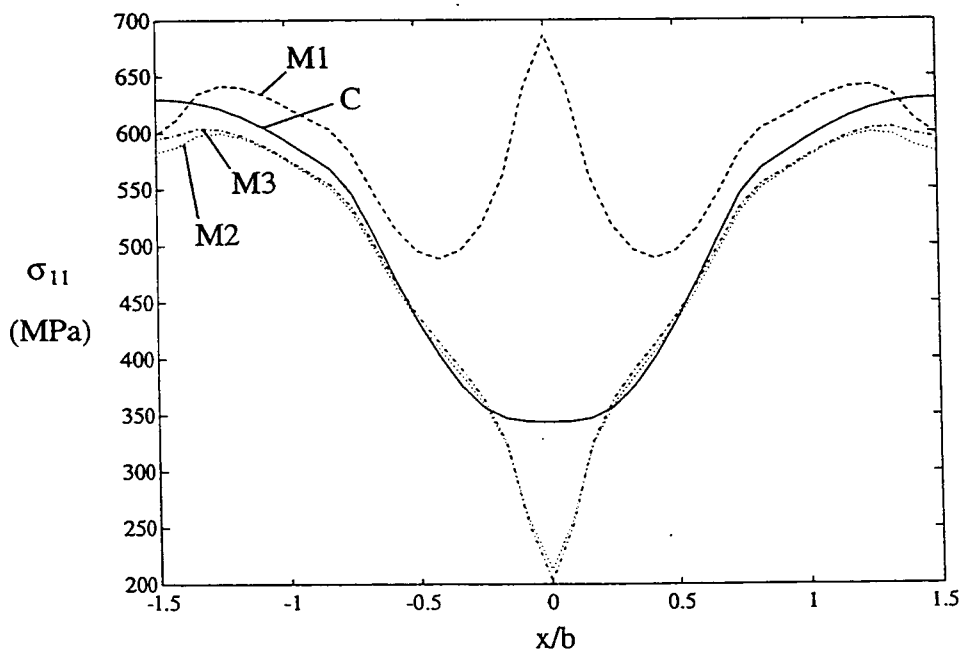

(b) FB4

Fig.11. Distribution of σ_{11} along the fiber boundries FB2 and FB4. Conventional FEM (C) and global/local method with 4-node macro elements (M1), 8-node macro elements (M2), and 12-node macro elements (M3) were used. The stress was transformed to the material coordinate systems.

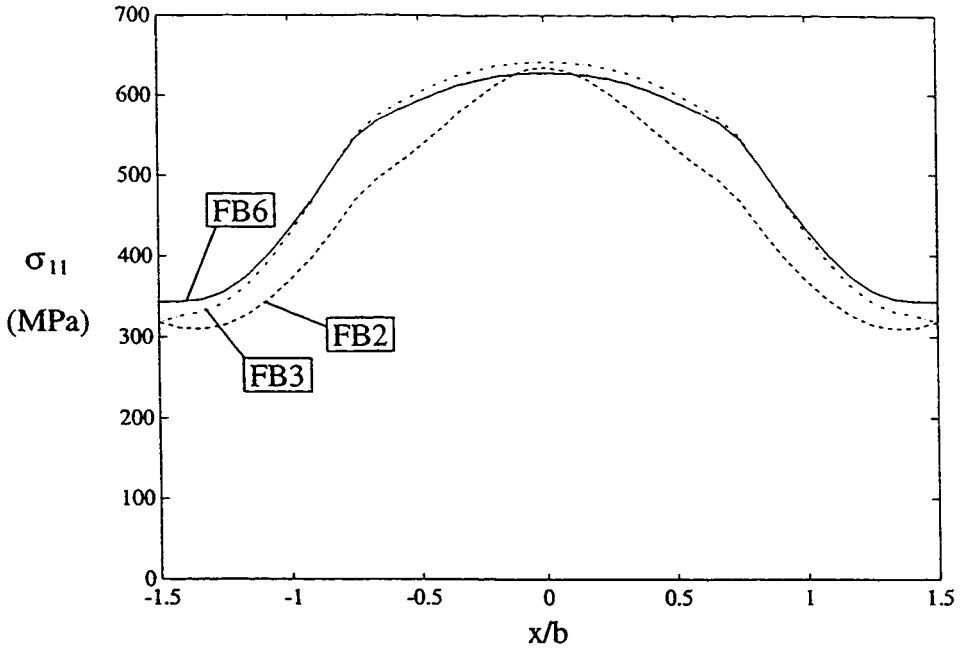

(a) σ_{11}

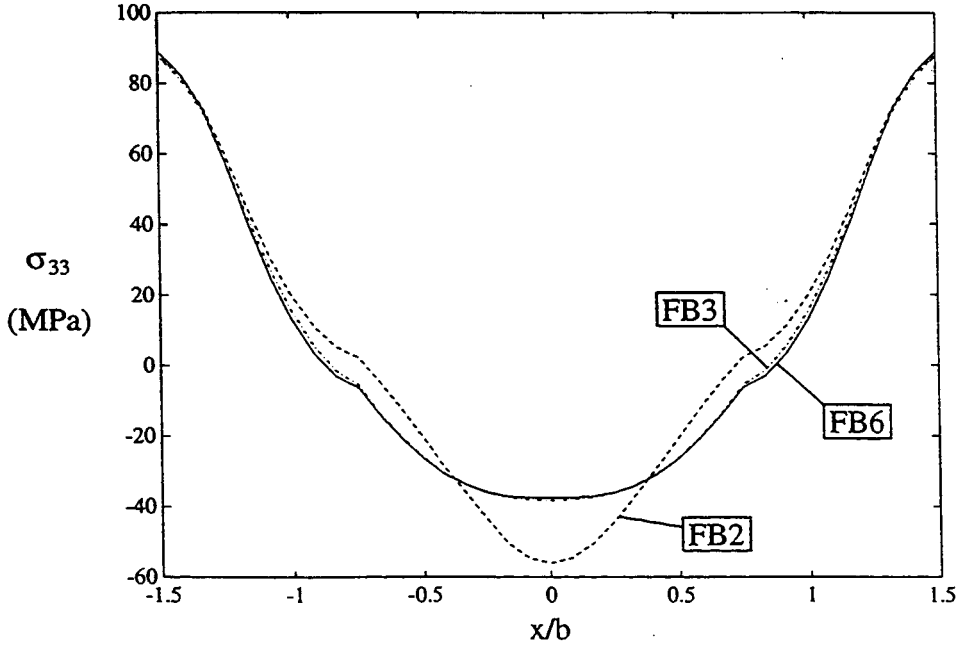

(b) σ_{33}

Fig. 12. Stress distributions along the fiber boundries FB2, FB3, and FB6. Global/local method with 12-node macro elements were used. The stresses were transformed to the material coordinate systems.

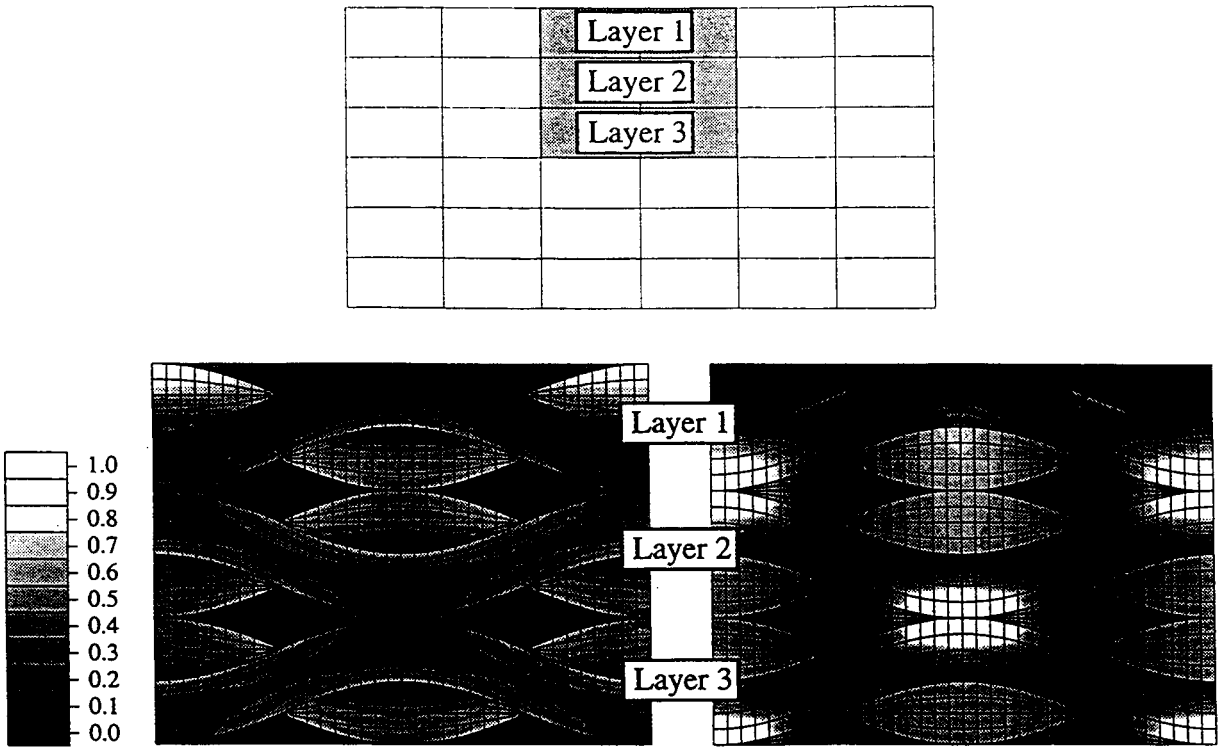

(a) σ_{11} /X (b) σ_{33} /Z

Fig. 13. Contour plots of normalized stresses for upper 3 mats. The stresses were transformed to the material coordinate systems and normalized by the strengths.

Boundary Effects in Woven Composites

John Whitcomb[1]
Gopal Kondagunta
Kyeongsik Woo

Texas A&M University
Aerospace Engineering Department
College Station TX 77843-3141 USA

Abstract

Two dimensional finite elements were used to study boundary effects in plain weave composite specimens subjected to extension, shear, and flexure loads. Effective extension, shear, and flexural moduli were found to be quite sensitive to specimen size. For extension and flexure loads stress distributions were affected by a free surface, but the free surface boundary effect did not appear to propagate very far into the interior. For shear load the boundary effect appeared to propagate much further into the interior.

Key Words: textiles
woven composites
finite elements
stress analysis
boundary effects

Introduction

Fiber tows, each consisting of thousands of individual filaments, can be woven, braided, knitted, etc. to create complex fiber preforms. These preforms are then impregnated with a resin and cured to make textile composites. The interlacing of the fiber bundles provides many obstacles to damage growth. Accordingly, there is the potential for greatly improved resistance to impact damage growth. Unfortunately, there are also negative effects due to the fiber tow interlacing. The fiber tow curvature reduces the effective in-plane moduli. The curvature also

---

[1] Correspondence and proofs should be send to Dr. John D. Whitcomb, Texas A&M University, Aerospace Engineering Department, College Station TX 77843-3141; telephone number: 409 845 4006.

induces many local stress concentrations which can result in early diffuse damage initiation, particularly in the matrix. The fabrication process is not benign. For example, weaving involves much mechanical handling of unprotected fibers (i.e. fibers which are not embedded in matrix). Stitching of textile preforms to increase delamination resistance has the side effects of breaking fibers and inducing local fiber curvature. Optimal design requires the capability to predict both the positive and negative effects of potential textile fiber architectures. Unfortunately, the complex fiber architecture is difficult to analyze. Accurate analysis requires accurate geometric representation and constituent properties, such as fiber and matrix properties and fiber volume percentage. For textile composites there is particular difficulty in determining the actual fiber tow geometry and developing a three-dimensional model which can be analyzed. There have only been a few attempts at detailed three dimensional analysis (eg. Refs. [1-3]). Even the accuracy of these models for local stress calculation is an open question because of the uncertainties in the input data (i.e. the approximation of tow geometry and other properties). Most of the analyses to date have been similar to laminate theory in level of approximation or detailed two dimensional (2D) or quasi-three-dimensional (Q3D) numerical analyses of a "representative" cross-section (eg. Refs. [4-7]). As the schematic in Figure 1 shows, there is no such "representative" cross-section, even for a plain weave composite. While such 2D or Q3D analyses are likely insufficient for accurate prediction of local stress states, they are useful for obtaining insight about the effects of fiber tow waviness on effective moduli and strengths. In fact, the results in this paper, which are based on 2D analyses, fall into this category.

The analysis of textile composites is in its infancy as compared to laminated composites. There are many aspects of the behavior of these materials which have not even been examined, much less accurately described. The objective of this paper is to begin to address one question

about the behavior of plain weave composites: "How does the presence of a boundary affect the stiffness and stress distribution in a representative unit cell?" The boundary surfaces referred to here are those present due to finite thickness. Three nominally simple boundary conditions were considered herein: in-plane extension, transverse shear, and flexure. Configurations of different thicknesses were analyzed using 2D finite elements. The analyses were performed using conventional elements and multi-field macro elements (reference 8). Macro elements are defined to be elements which contain internal microstructure. The multi-field elements are a form of reduced substructuring. The macro elements permitted analysis of quite large models without requiring huge amounts of computer memory and cpu time. Of course, a few macro elements are not as accurate as using a huge collection of conventional elements. Accordingly, one additional objective of the paper is to evaluate the performance of macro elements for simple configurations.

The following sections will begin with a discussion of the configurations studied. Then the results will be discussed. First effective extensional, shear, and flexural moduli will be discussed. Then the effects of boundaries on stress distributions will be discussed.

Configurations

The various configurations studied are all synthesized from a single basic unit cell. This unit cell will be discussed first. Then boundary conditions for infinite and finite configurations will be discussed.

Unit Cell

The basic unit cell is shown in Figure 2 . The cell consists of tows running in the x- and z- directions. In reality there would also be pure matrix pockets, but these were filled with z-

direction tows in the model used. (Of course, in reality there is no typical cross section either, as discussed earlier.) The two dimensional approximation implies that the x- direction tow is a wavy "plate" and the z-direction tows are straight fiber bundles. Obviously these are serious approximations, so the results presented are intended to be qualitative only. The centerline of the x-direction tows follows a wavy path described by the function $\frac{\beta}{4}\sin\frac{\pi x}{\alpha}$. For the results presented herein $\alpha=1.5\beta$. The thickness of the tow as measured along a line normal to the tow centerline was held constant. It should be noted that the unit cell selected assumes a symmetric stacking of the woven mats. There are an infinite number of other possibilities.

Two sets of two material properties were used. They are

Set I

E_{11} = 100 GPa	E_{22} = 10 GPa	E_{33} = 10 GPa
ν_{12} = 0.35	ν_{13} = 0.35	ν_{23} = 0.3
G_{12} = 5 GPa	G_{13} = 5 GPa	G_{23} = 3.845 GPa

Set II

E_{11} = 165.8 GPa	E_{22} = 11.51 GPa	E_{33} = 11.51 GPa
ν_{12} = 0.273	ν_{13} = 0.273	ν_{23} = 0.33
G_{12} = 15.4 GPa	G_{13} = 15.4 GPa	G_{23} = 4.17 GPa

These properties were transformed to account for the waviness of the x-direction tow. Plane strain conditions were imposed to obtain two dimensional properties. Two sets of properties were used. This is admittedly not optimal. The homogenization analyses were performed using Set I. The stress analysis results were obtained using Set II.

Periodic Boundary Conditions for Infinite Configurations

Figure 2 shows a typical unit cell for symmetrically stacked mats before deformation. If this cell is imbedded within an infinite array of identical cells and displacements or tractions are imposed "at infinity", then every unit cell will deform identically. The periodicity of the displacement field can be imposed on a single unit cell, thus permitting the solution for the infinite domain. The solution for an infinite domain will be useful for comparison with finite configurations subjected to nominally uniform extension or shear. Using the coordinate system in Figure 2a, the periodic conditions can be expressed as

$$u(\alpha,y) = u(-\alpha,y) + u_2 - u_1 \tag{1}$$

$$v(\alpha,y) = v(-\alpha,y) + v_2 - v_1 \tag{2}$$

$$u(x,\beta) = u(x,-\beta) + u_4 - u_1 \tag{3}$$

$$v(x,\beta) = v(x,-\beta) + v_4 - v_1 \tag{4}$$

There are no specified non-zero forces (The net forces are zero at any point inside the infinite media.). The "load" consists of the values chosen for $(u_2 - u_1)$, $(v_2 - v_1)$, etc. These values depend on the nominal strain state desired. (Specific values for the different states will be discussed later in this section. Equations 1-4 impose certain constraints which are not so obvious, but are worth mentioning, since they are exploited in the finite element analysis. These constraints are

$$u_3 - u_4 = u_2 - u_1 \tag{5}$$

$$v_3 - v_2 = v_4 - v_1 \tag{6}$$

$$u_3 - u_2 = u_4 - u_1 \tag{7}$$

$$v_3 - v_4 = v_2 - v_1 \tag{8}$$

These constraints can be obtained from equations 1-4 by substituting in specific vertex values of x and y. For example, substitute $x=\alpha$ into equation 3.

$$u(\alpha,\beta) = u(\alpha, -\beta) + u_4 - u_1$$

But $u(\alpha,\beta) = u_3$ and $u(\alpha, -\beta) = u_2$. Hence, equation 3 states that $u_3 - u_2 = u_4 - u_1$. Equations 5-8 indicate that if the nodal displacements at the four corners of the unit cell are used to calculate the displacement gradients, we find that $\left(\frac{\partial u}{\partial x}\right)_0, \left(\frac{\partial v}{\partial x}\right)_0, \left(\frac{\partial u}{\partial y}\right)_0$, and $\left(\frac{\partial v}{\partial y}\right)_0$ are constant. The subscript "0" is used to indicate that these are nominal displacement gradients. On a pointwise basis these are certainly not constant for the obviously inhomogeneous unit cells. Equations 1-4 can now be expressed as

$$u(\alpha,y) = u(-\alpha,y) + 2\alpha\left(\frac{\partial u}{\partial x}\right)_0 \tag{9}$$

$$v(\alpha,y) = v(-\alpha,y) + 2\alpha\left(\frac{\partial v}{\partial x}\right)_0 \tag{10}$$

$$u(x,\beta) = u(x, -\beta) + 2\beta\left(\frac{\partial u}{\partial y}\right)_0 \tag{11}$$

$$v(x,\beta) = v(x, -\beta) + 2\beta\left(\frac{\partial v}{\partial y}\right)_0 \tag{12}$$

Because of symmetries only part of the unit cell must be modeled. Herein the quarter unit cell shown in Figure 2(b) was modeled. If all the symmetries had been exploited, only one-eighth of the unit cell would have to be modeled. For convenience the coordinate system is shifted to the center in Figure 2(b).

For extension loading the boundary conditions are quite simple. The constraints imposed for nominal σ_x loading are

$$\begin{aligned} u\left(-\frac{\alpha}{2}, y\right) &= 0 \qquad u\left(\frac{\alpha}{2}, y\right) = \text{specified constant value} \\ v\left(x, -\frac{\beta}{2}\right) &= 0 \qquad v\left(x, \frac{\beta}{2}\right) = \text{constant, but unknown} \end{aligned} \tag{13}$$

Nominal σ_y loading (which was not considered herein) would be very similar. For nominal σ_{xy} load the boundary conditions are

$$\begin{aligned} u\left(x, \frac{-\beta}{2}\right) &= -u\left(x, \frac{\beta}{2}\right) = \text{specified constant value} \\ v\left(\frac{-\alpha}{2}, y\right) &= -v\left(\frac{\alpha}{2}, y\right) = \text{specified constant value} \\ u\left(\frac{-\alpha}{2}, -y\right) &= -u\left(\frac{\alpha}{2}, y\right) \\ v\left(-x, \frac{-\beta}{2}\right) &= -v\left(x, \frac{\beta}{2}\right) \end{aligned} \tag{14}$$

The boundary conditions in equations 14 state that the displacements normal to an edge are anti-symmetric (and unknown except at the vertices). The tangential displacements are constant along an edge and are specified.

Boundary Conditions for Finite Configurations

Extension, shear, and flexure loading were considered for a wide range of specimen thickness (in the y-direction). Hence, the various meshes had different numbers of unit cells. For extension loads the boundary conditions were like those in equation 13 if one considers α

and β to be the dimensions of the entire mesh, rather than just a quarter unit cell except that the top surface was traction free. Hence, the normal displacement "v" was not constrained to be constant along the top. For shear load all boundary displacements were constrained to follow the deformation u = cy and v = cx. Consequently, the boundaries remained straight after deformation for shear loading.

For flexure loads the top and bottom surfaces of the model were traction free. A linear variation of normal displacements were imposed on left and right ends of the model.

Results and Discussion

There are two types of results which will be discussed. The first will illustrate the effect of specimen thickness on effective moduli. The second will illustrate the effect of unit cell location on stress distributions.

Effective Moduli

For nominally simple deformation states, the effective engineering properties are expected to converge to constant values as the specimen thickness increases. Figure 3 shows the variation of the normalized effective E_x. Figure 3a shows the variation of the average E_x with the number of unit cells. The E_x is normalized by the E_x for an infinite array of unit cells modeled using conventional finite elements. The three curves were obtained using conventional finite elements and 8-node and 12-node multi-field macro elements. The 8-node macro element must be inherently a little too stiff, since it converges to a value approximately one percent too large. The 12-node macro element agrees very well with the conventional finite element results. For 8 unit cells through the thickness the effective E_x is within about one percent of convergence. This indicates that a specimen would need to be 8 unit cells thick to give an effective E_x within

one percent of a very thick specimen. Figure 3b shows the variation of the effective E_x with position for a configuration which has eight unit cells through the thickness. The effective E_x for each quarter unit cell was calculated based on the strain energy in the region. This is not a rigorous definition, but it does offer some insight. The figure shows that the boundary quarter unit cell is about 18 percent softer than an interior quarter unit cell. The next quarter unit cell is about 5 percent too stiff. The third quarter unit cell has almost exactly the same stiffness as cells which are much further from the boundary. There is an obvious boundary effect, but it dies out very quickly.

Figure 4 shows the effect of model size on normalized effective shear modulus G_{xy}. In contrast to E_x, the shear modulus converges from the stiff side. This difference is a consequence of the boundary conditions imposed. For E_x there were free surfaces. The traction free condition permitted warping deformation to occur more easily near the free surface than in the interior, so the boundary caused softening. In contrast, all of the finite size shear specimens had specified x- and y- displacements over the entire boundary. This fully constrained boundary deformation resulted in larger effective G_{xy} for smaller specimens. Figure 4 also shows that 8-node macro elements perform poorly in shear. The 12-node macro elements perform quite well. It is interesting to note the distribution of the strain energy in a finite size shear model. The bar chart in Fig. 5 shows the strain energy in each quarter unit cell for a 3x3 array of unit cells. The effect of the boundary on the strain energy distribution is obviously quite complex.

Figure 6 shows the variation of normalized flexural modulus with model size. The flexural modulus is defined to be (flexural stiffness)/I, where I = the second moment of the area. The flexural modulus in Figure 6 is normalized by the value for a configuration which is

ten cells thick. The flexural modulus converges more slowly than the extensional modulus. The 12-node macro element performs very well. The 8-node macro element is a little too stiff.

Stress Distributions

Figures 7-9 illustrate the effect of a free surface on stress distributions. Distributions are shown for extension, shear, and flexure. The stresses shown are evaluated with respect to the xy (global) coordinate system.

Figure 7 shows the stress distributions for extension loading for three unit cells from two different configurations. One configuration had two unit cells through the thickness. The other had six unit cells through the thickness. The locations of the unit cells considered are indicated by shading in the figures. The waviness of the x-direction tow and the inhomogeneity causes a complicated variation of all three stresses. The σ_x variation in the longitudinal tow is dominated by flexure induced by tow straightening, as shown by the locations of maximum and minimum σ_x. The σ_y is largest where the tows contact. The σ_{xy} is largest where the tow rotation is largest.

There are both striking similarities and differences in the stress distributions for the three unit cells. Figure 7 shows that the interior and exterior unit cells have very different stress distributions. There is obviously a significant free surface effect. The exterior unit cells in Figure 7 have very similar distributions for all three stress components. This suggests that for extension load the response of the exterior unit cells is not very sensitive to the total specimen thickness.

The interior unit cell exhibits almost the same symmetries that one would expect from a cell embedded inside an infinite array. Also, the interior half of the exterior unit cells has stress distributions which are very close to those for the lower half of the interior unit cell. Apparently the free surface effect does not propagate very far into the interior.

Figure 8 shows the stress distributions for shear loading. Single unit cell and 3x3 unit cell configurations were studied. Only the σ_y and σ_{xy} distributions are shown, since σ_x was quite small. In this case there are no free surfaces. (Displacements were specified along the entire boundary.) As was the case for extension, the interior and exterior response is different. The interior unit cell is located in the middle of the finite element model. Hence, the symmetries exhibited by the interior cell do not indicate the attenuation of boundary effects. In contrast to extension load, Figure 8 shows that for shear load the response of the boundary unit cells is very sensitive to total specimen size. Further studies are needed to determine the boundary layer thickness for shear loads.

Figure 9 shows stress distributions for flexure loads. Only exterior unit cells are compared. The single unit cell model was subjected to a combination of extension and flexure so that the loading would be comparable to the exterior unit cell of the thicker model. The thicker model was subjected to pure flexure. Both models have free surfaces at both the top and bottom. The maximum σ_x does not occur at the free surface. This is because local flexure of the wavy fiber tow as it tries to straighten attenuates the σ_x. The top halves of the two unit cells in Figure 9 have very similar σ_x, σ_y, and σ_{xy} distributions. The lower halves exhibit much more differences. This is not surprising since the lower surface of the single cell is traction free but the lower surface of the cell from the thicker model is not. These results further indicate that there is a free surface effect (in this case, from the lower surface of the single unit cell model), but that the boundary layer is quite small. Finally, it should be noted that the stresses were lower for the flexure case than for the extension case even though the maximum nominal axial strain was .001 for both.

Conclusions

Boundary effects were studied for woven composites subjected to in-plane extension, shear, and flexure. Effective moduli and stress distributions were calculated for configurations ranging from very thin to very thick. Only two dimensional models were studied. Since woven textiles are really three dimensional, these two dimensional results should only be interpreted qualitatively. Boundary effects were significant both in terms of stiffness and stresses. A specimen thickness of 6-8 unit cells was required to obtain moduli within about 2% of that for very thick specimens. For extension and flexure loading the stress distribution in exterior unit cells were quite insensitive to total specimen thickness. There appeared to be a characteristic response of boundary cells. Also, the boundary effect did not propagate very far into the interior. The response for shear load was more complex than for extension and flexure. Further work is needed to characterize boundary effects for shear loads.

References

1. Whitcomb, J.D. "Three-Dimensional Stress Analysis of Plain Weave Composites," in *Composite Materials: Fatigue and Fracture (Third Volume), ASTM STP 1110*, T.K. O'Brien, Ed., Philadelphia: American Society for Testing and Materials, pp. 417-438.
2. Paumell, P., A. Hassim, and F. Léné. La Recherche Aérospatiale, 1:1-12 (1990).
3. Paumell, P., A. Hassim, and F. Léné. La Recherche Aérospatiale, 6:47-62 (1991).
4. Ishikawa, T. Fiber Science Technology, 15:127-145 (1981).
5. Ishikawa, T., and T.-W. Chou, J. Material Science, 17:3211-3220 (1982).
6. Kriz, R.D., J. Composites Technology & Research, 7:55-58 (1985).

7. Avery, W.B., and C.T. Herakovich. A Study of the Mechanical Behavior of a 2D Carbon-Carbon Composite, Virginia Polytechnic Institute and State University, Interim Report 66 (1987).

8. Whitcomb, J.D., and K. Woo. "Enhanced Direct Stiffness Method for Finite Element Analysis of Textile Composites," *CMC Report No. 92-17*, Texas Engineering Experiment Station, Texas A&M University, (1992); submitted for publication in Journal of Composite Materials.

Figure Captions

Figure 1. Variation of cross section with location.

Figure 2. Basic two-dimensional unit cell models.

Figure 3. Normalized extensional modulus E_x. Eight-node traditional elements were used for the infinitely repeating unit cell case.

(a) Average normalized E_x vs. number of unit cells through thickness.

(b) Normalized extensional modulus vs. position in an 8-unit cell configuration (The sketch only shows four unit cells, since the configuration is symmetric.)

Figure 4. Normalized shear modulus vs. number of unit cells through the thickness of the configuration. (The number of unit cells is the same in both the x- and y-directions.)

Figure 5. Normalized strain energy distribution in 3x3 unit cell model subjected to shear load. Strain energy in each quarter unit cell is normalized by that for an infinitely repeating unit cell array subjected to shear.

Figure 6. Normalized flexural modulus vs. number of unit cells through the thickness of the configuration. Results were normalized with the flexural modulus for a ten unit cell model.

Figure 7. Stress contours for a two-dimensional model of a plain weave composite under extension (nominal axial strain = .001).

(a) Axial Stress

(b) Transverse Stress

(c) Shear Stress

Figure 8. Stress contours for a two-dimensional model of a plain weave composite under shear (nominal shear strain = .001).

(a) Transverse Stress

(b) Shear Stress

Figure 9. Stress contours for a two-dimensional model of a plain weave composite under bending (nominal axial strain at top surface = .001).

(a) Axial Stress

(b) Transverse Stress

(c) Shear Stress

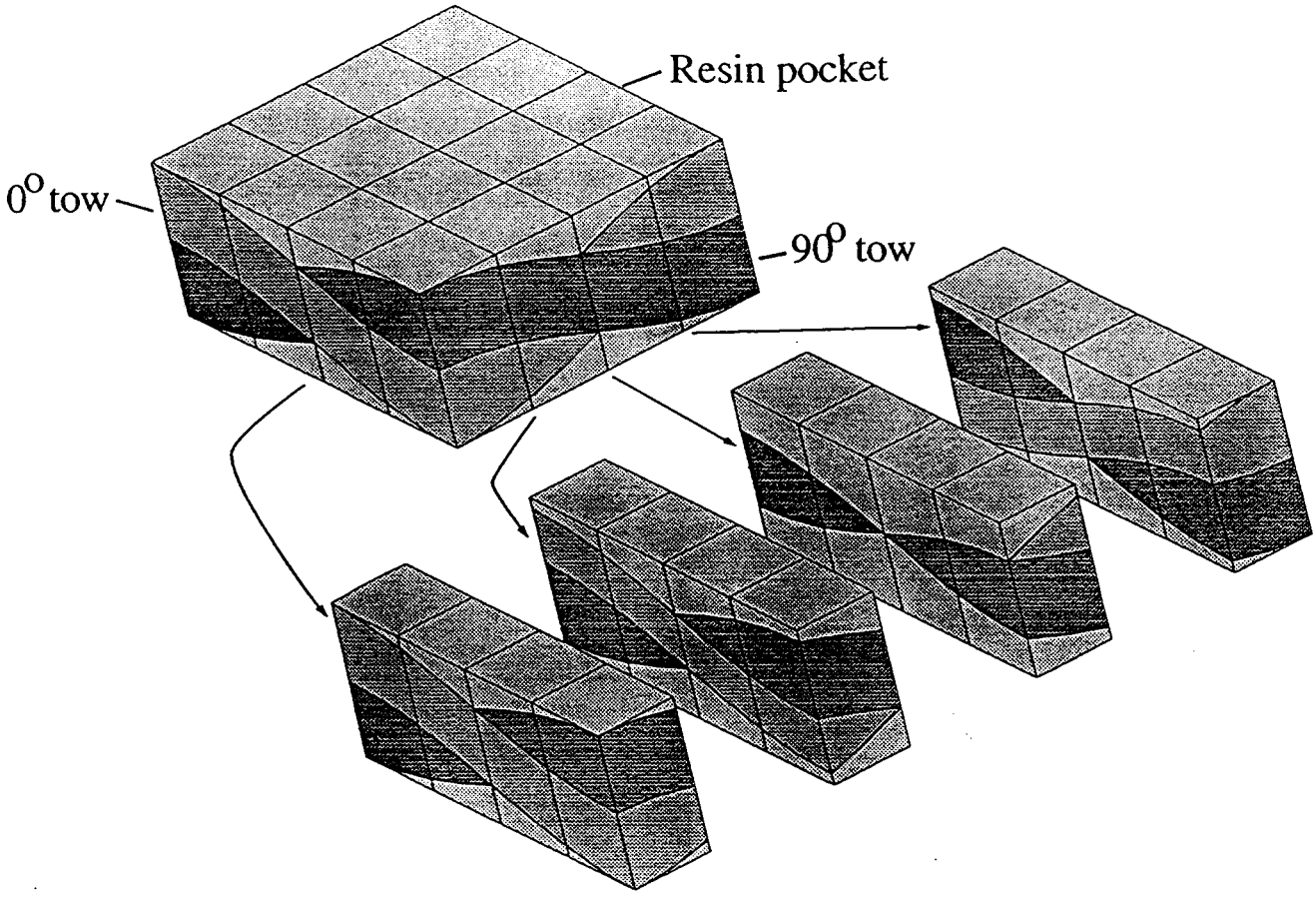

Figure 1 Variation of cross section with location.

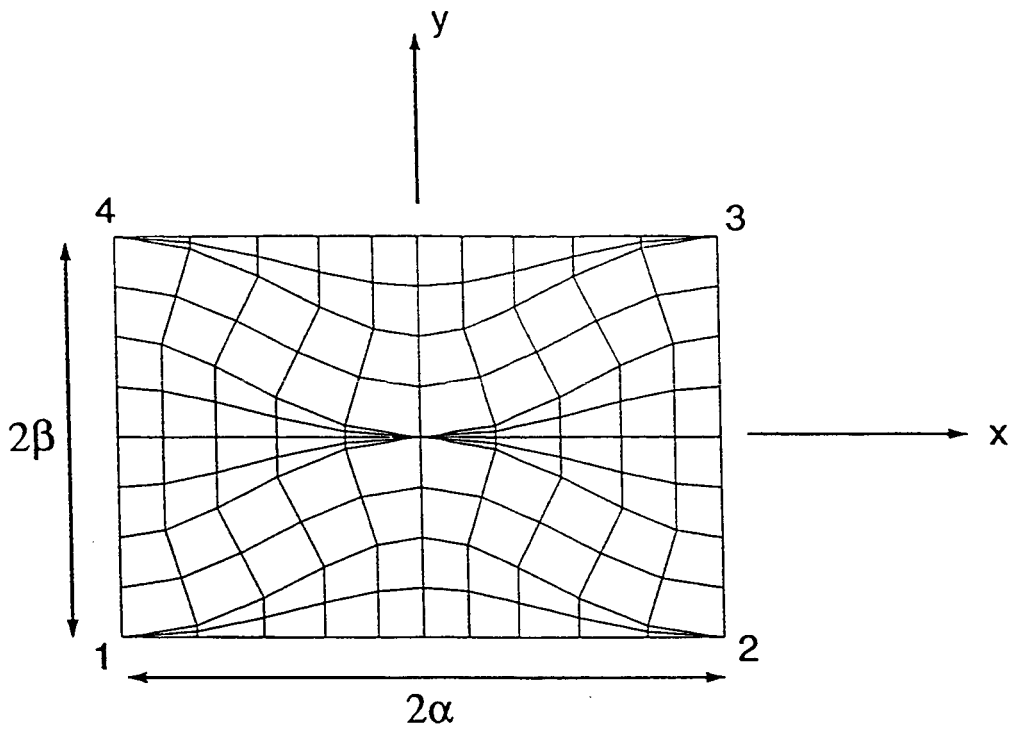

(a) Full unit cell

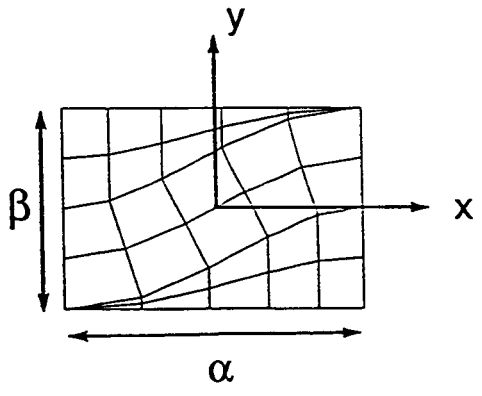

(b) Quarter unit cell

Figure 2 Basic two-dimensional unit cell models.

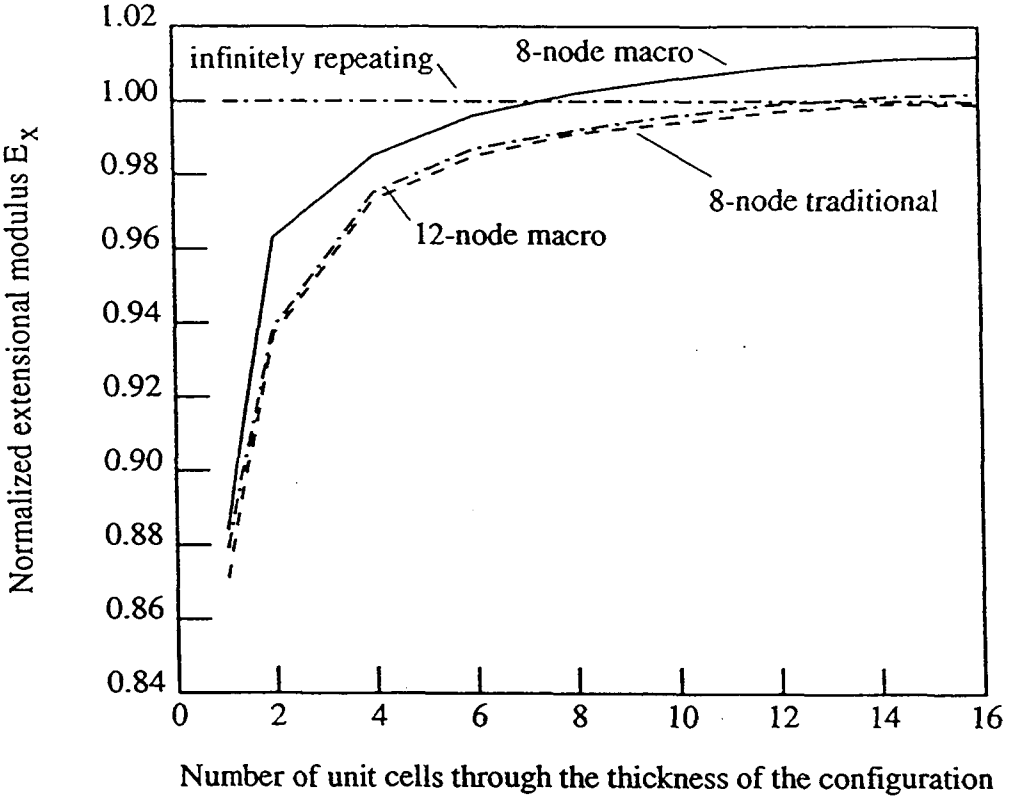

(a) Average normalized E_x vs number of unit cells through thickness.

Fig. 3 Normalized extensional modulus E_x. Eight-node traditional elements were used for the infinitely repeating unit cell case.

exdata

/Users/whit/Papers/Boundary/BoundaryEffects/xyplot/extension/ex.topdraw

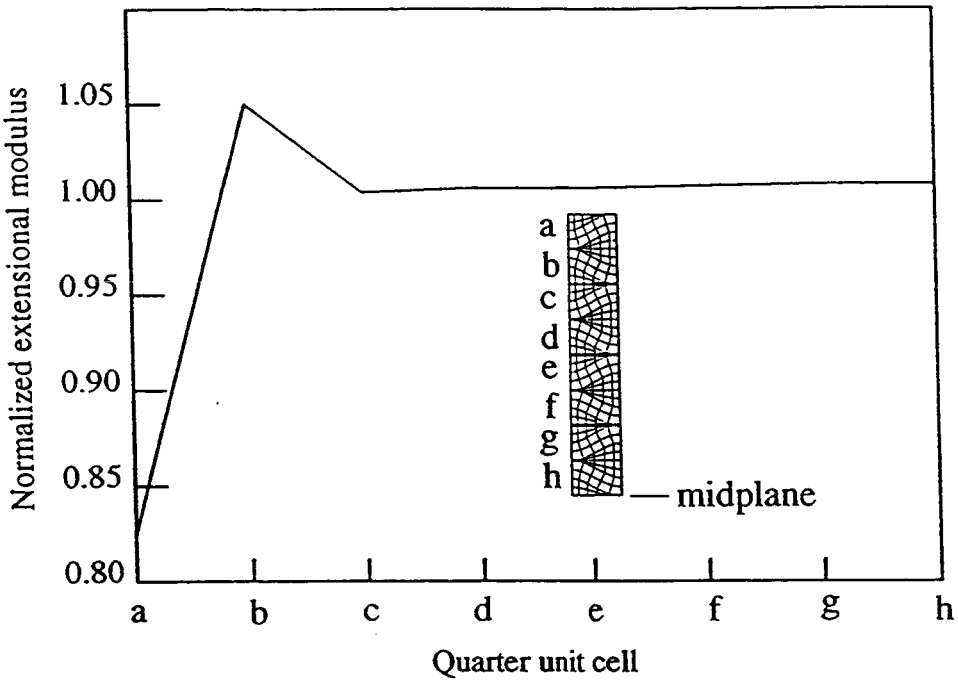

(b) Normalized extensional modulus vs. position in an 8-unit cell configuration. (The sketch only shows four unit cells, since the configuration is symmetric.)

Figure 3, completed.

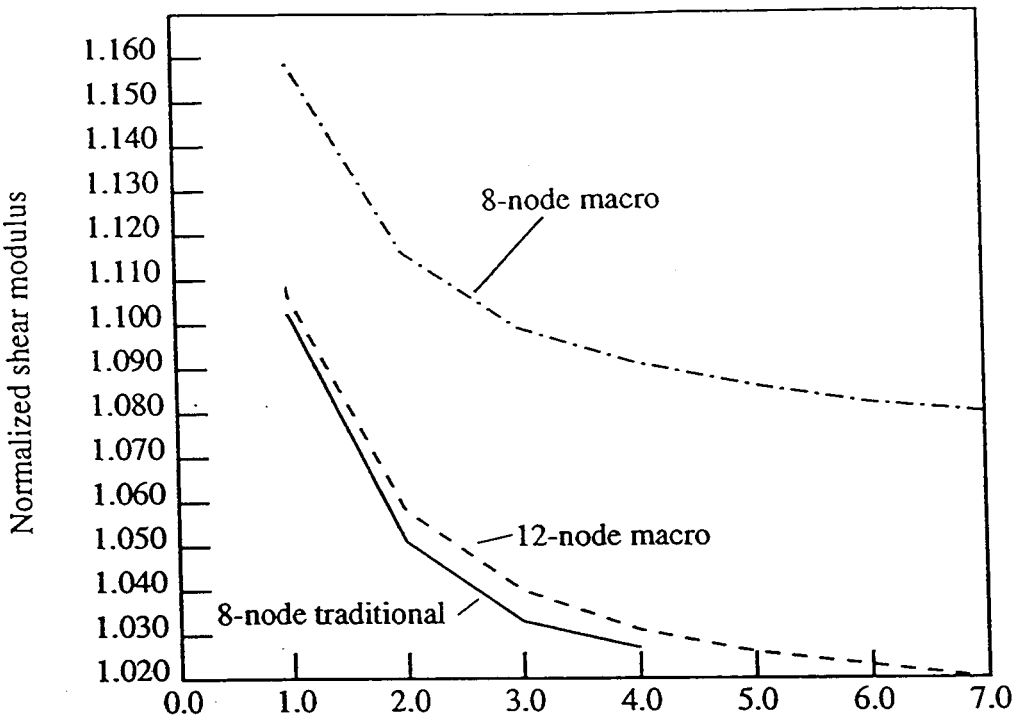

Fig. 4 Normalized shear modulus vs. number of unit cells through the thickness of the configuration.(The number of unit cells is the same in both the x- and y- directions).

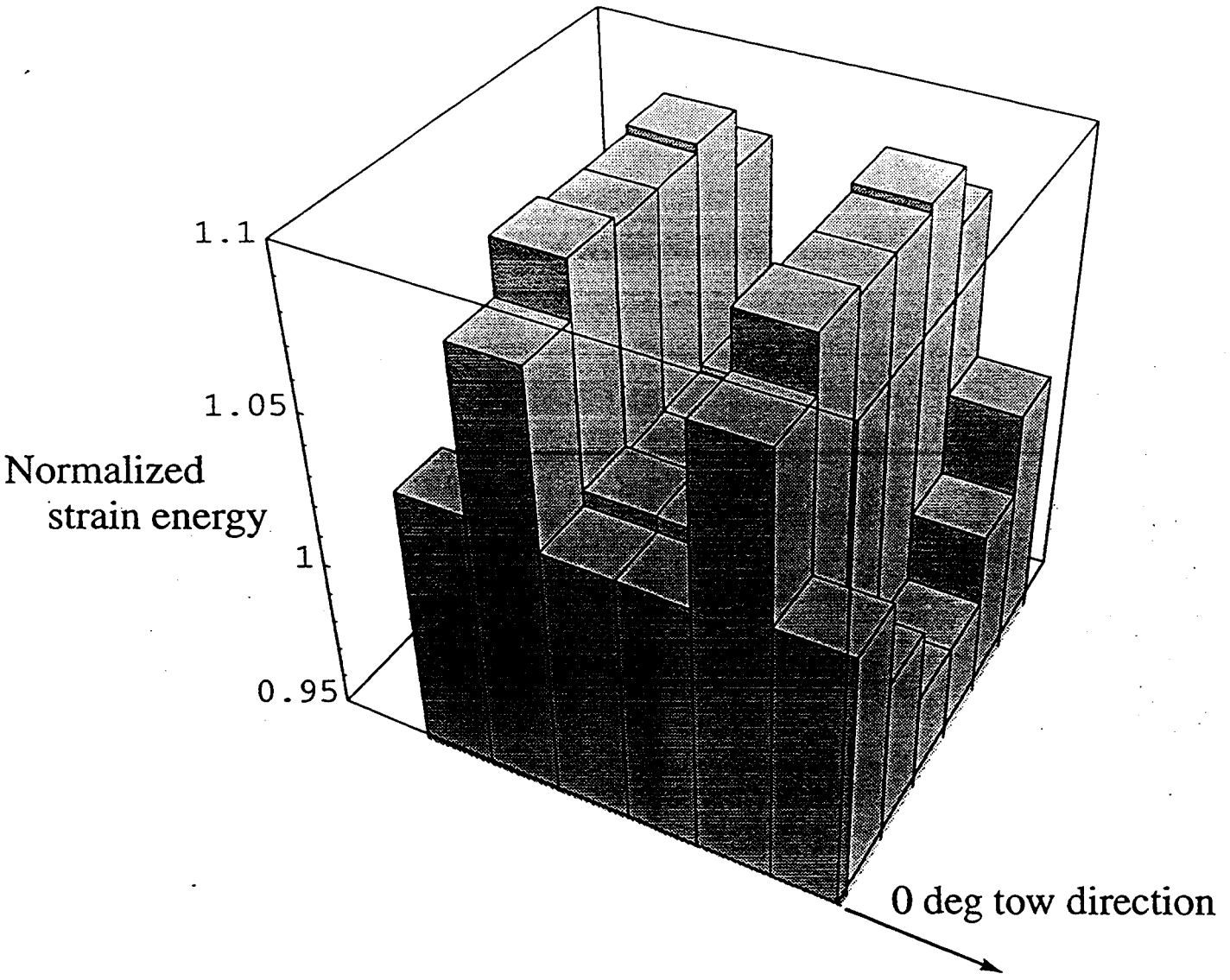

Figure 5 Normalized strain energy distribution in 3x3 unit cell model subjected to shear load. Strain energy in each quarter unit cell is normalized by that for an infinitely repeating unit cell array subjected to shear.

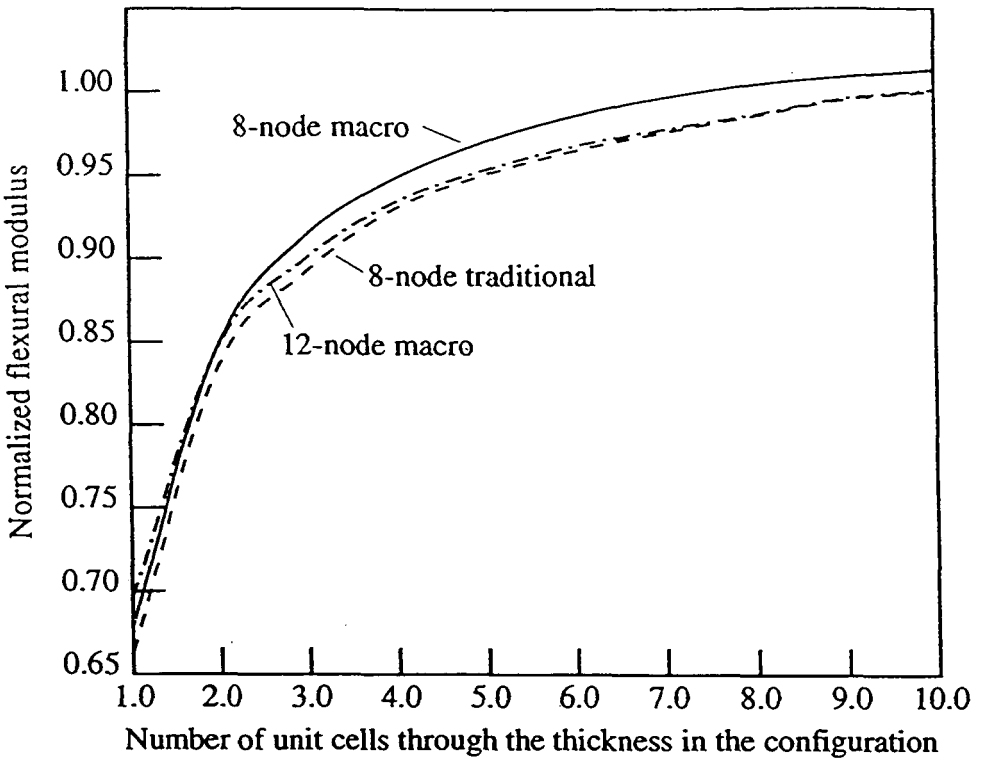

Fig. 6 Normalized flexural modulus vs. number of unit cells through the thickness of the configuration. Results were normalized with the flexural modulus for a ten unit cell model.

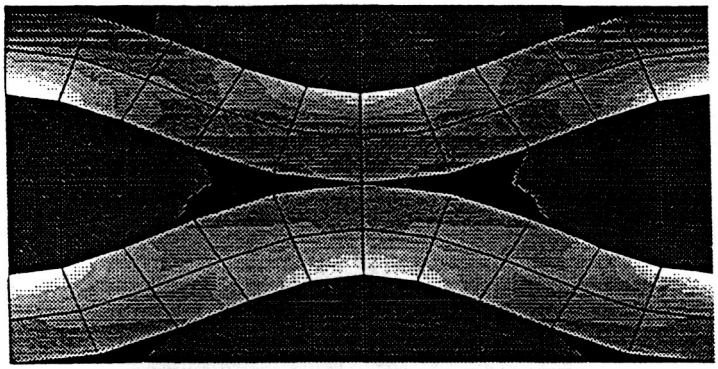

(i) Top unit cell of model with two unit cells through thickness.

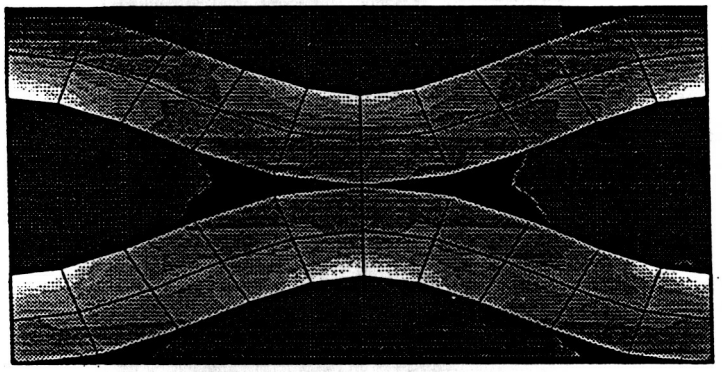

(ii) Exterior unit cell of model with six unit cells through thickness.

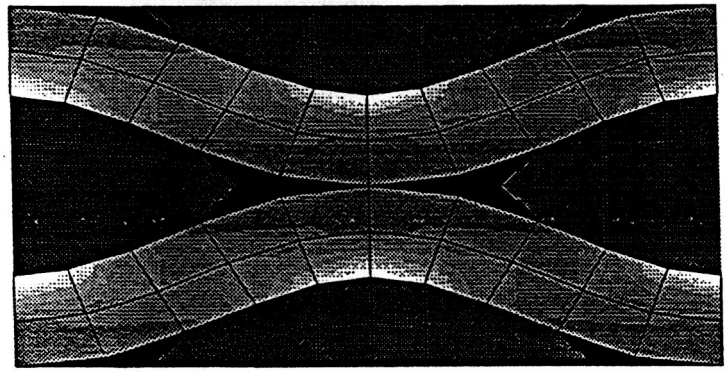

(iii) Interior unit cell of model with six unit cells through thickness.

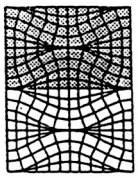

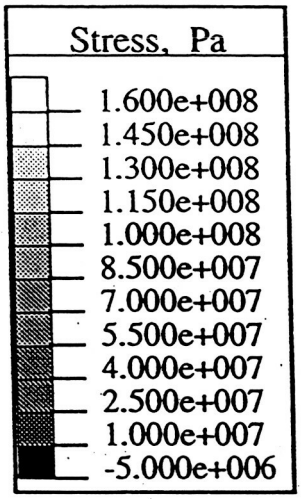

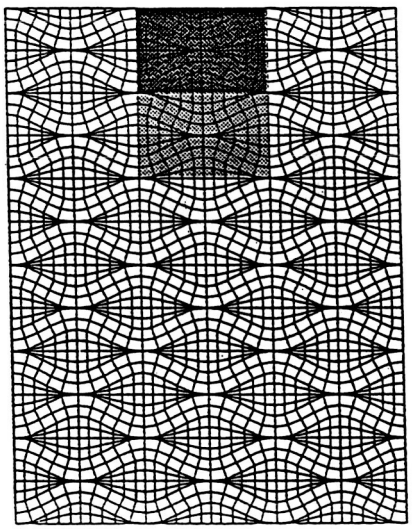

(a) Axial Stress

Figure 7 Stress contours for a two dimensional model of a plain weave composite under extension (nominal axial strain = .001).

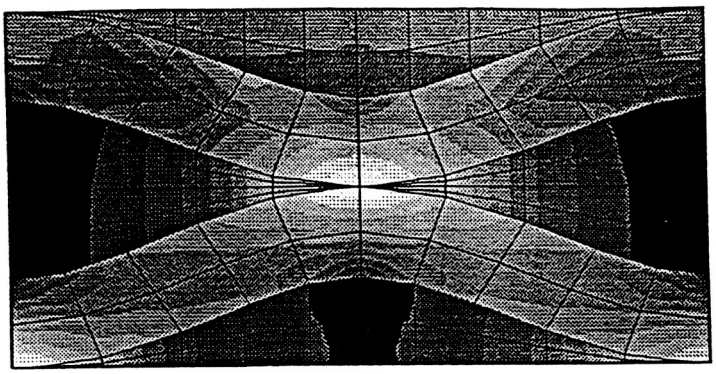

(i) Top unit cell of model with two unit cells through thickness.

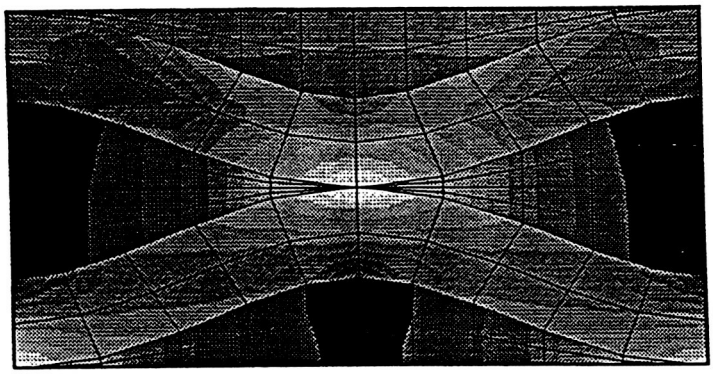

(ii) Exterior unit cell of model with six unit cells through thickness.

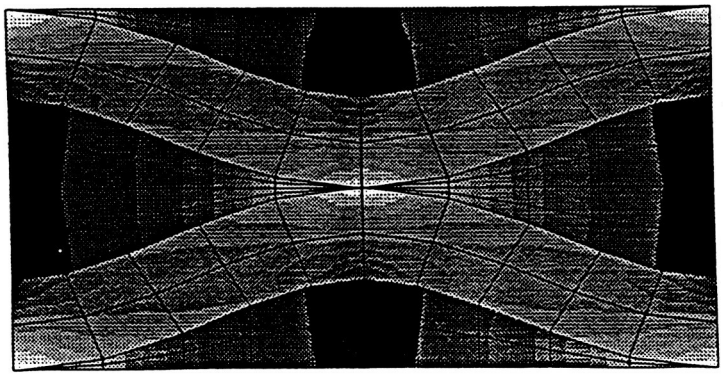

(iii) Interior unit cell of model with six unit cells through thickness.

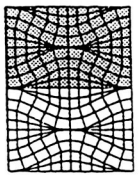

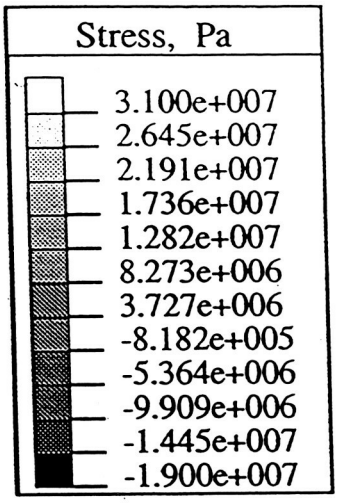

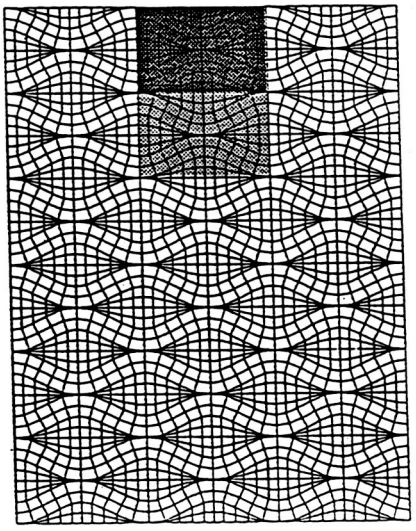

(b) Transverse Stress

Figure 7, Continued.

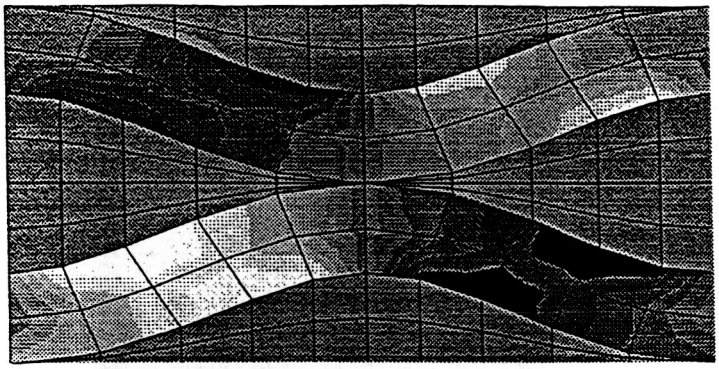

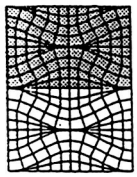

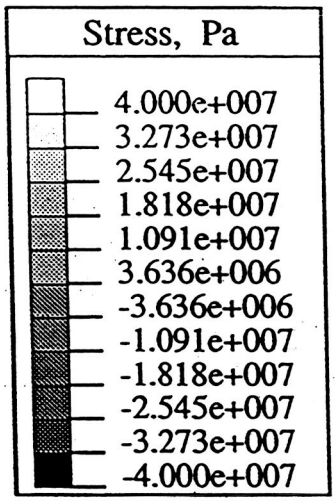

(i) Top unit cell of model with two unit cells through thickness.

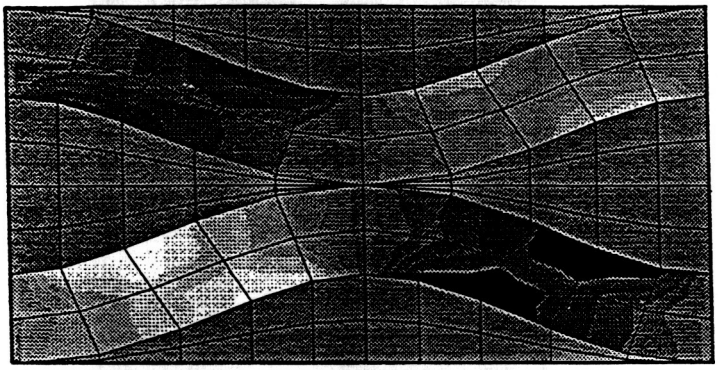

(ii) Exterior unit cell of model with six unit cells through thickness.

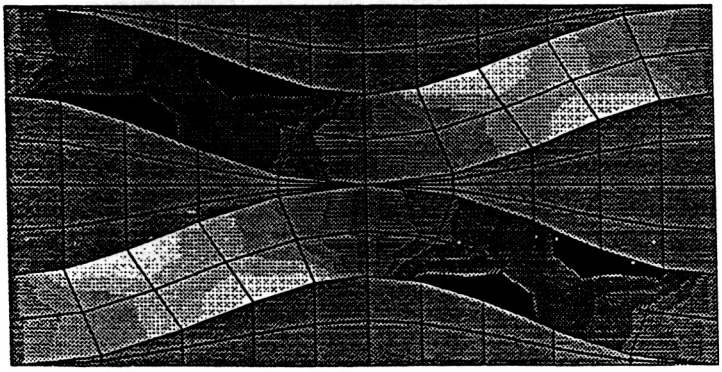

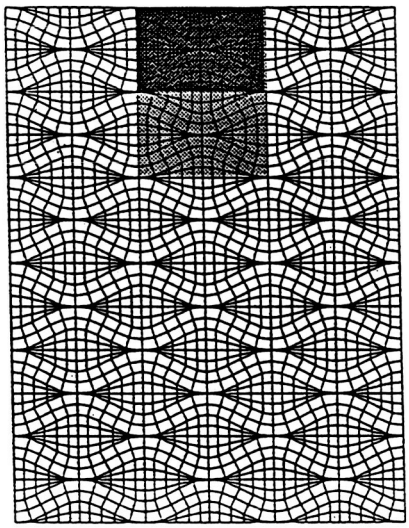

(iii) Interior unit cell of model with six unit cells through thickness.

(c) Shear Stress

Figure 7, Concluded.

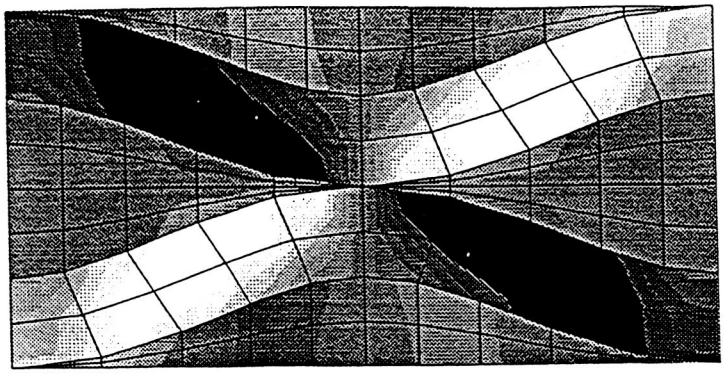

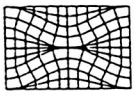

(i) Single Unit Cell

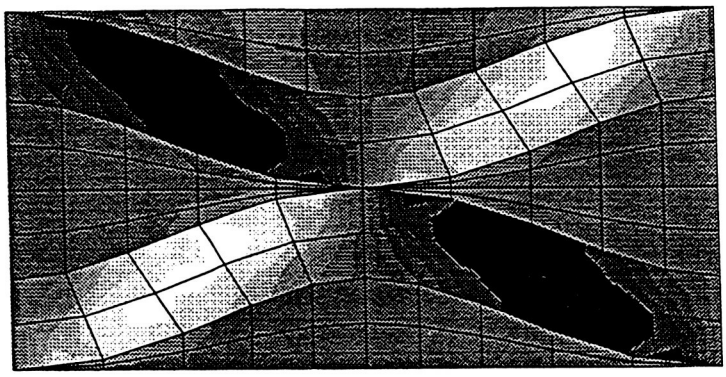

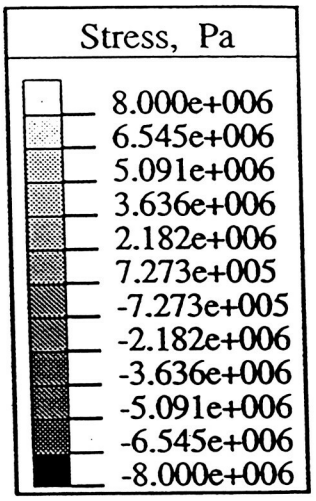

(ii) Exterior Unit Cell of a (3x3) unit cell model

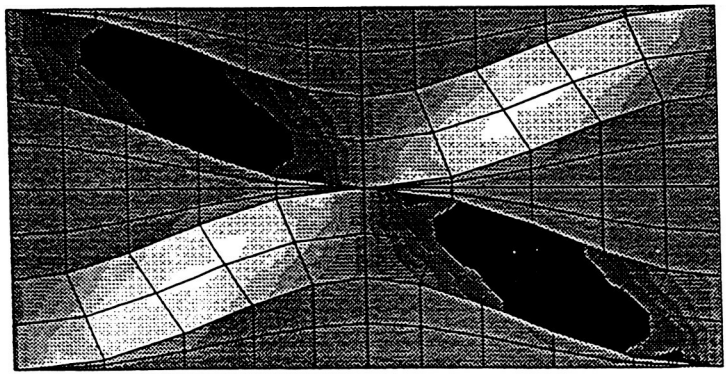

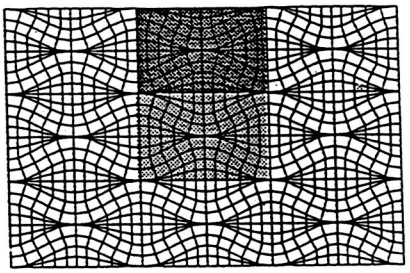

(iii) Interior Unit Cell of a (3x3) unit cell model

(a) Transverse Stress

Figure 8 Stress contours for a two dimensional model of a plain weave composite under shear. (nominal shear strain = .001)

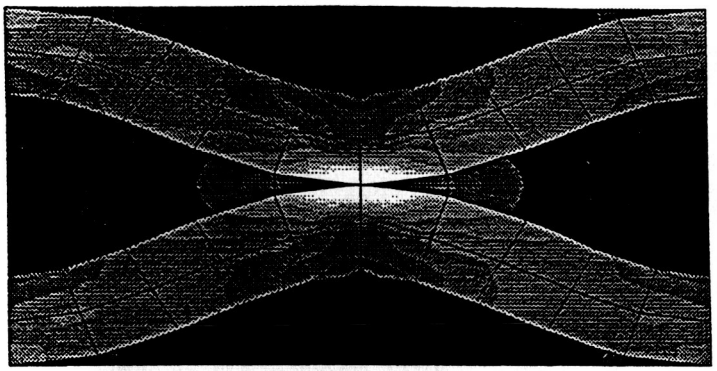

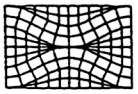

(i) Single Unit Cell

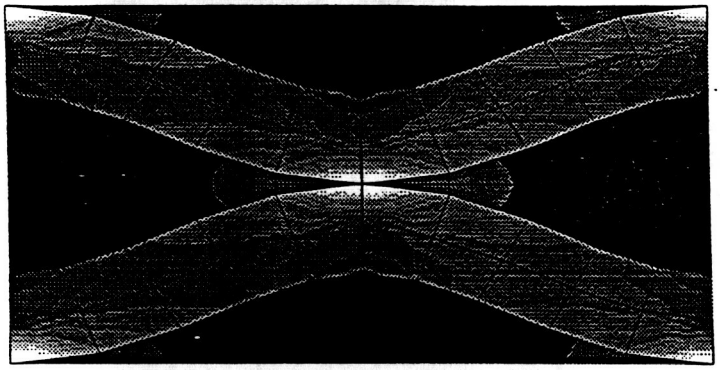

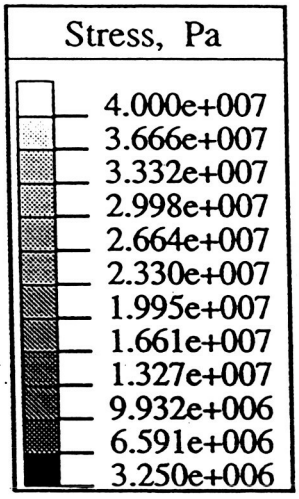

(ii) Exterior Unit Cell of a (3x3) unit cell model

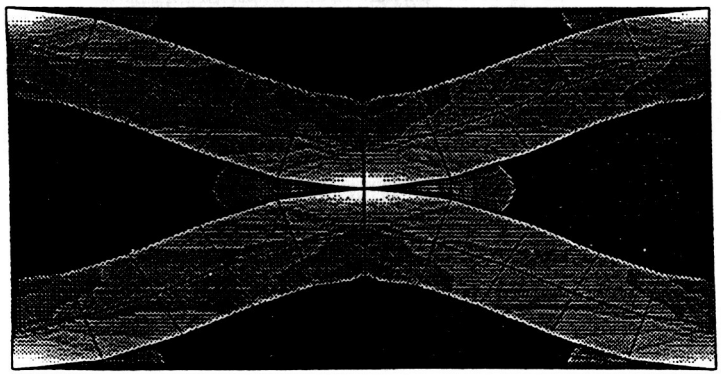

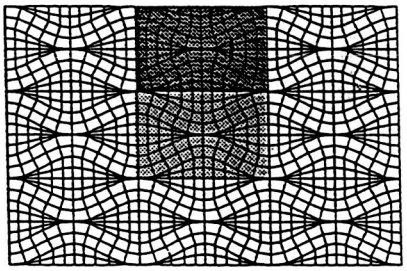

(iii) Interior Unit Cell of a (3x3) unit cell model

(b) Shear Stress

Figure 8, Concluded.

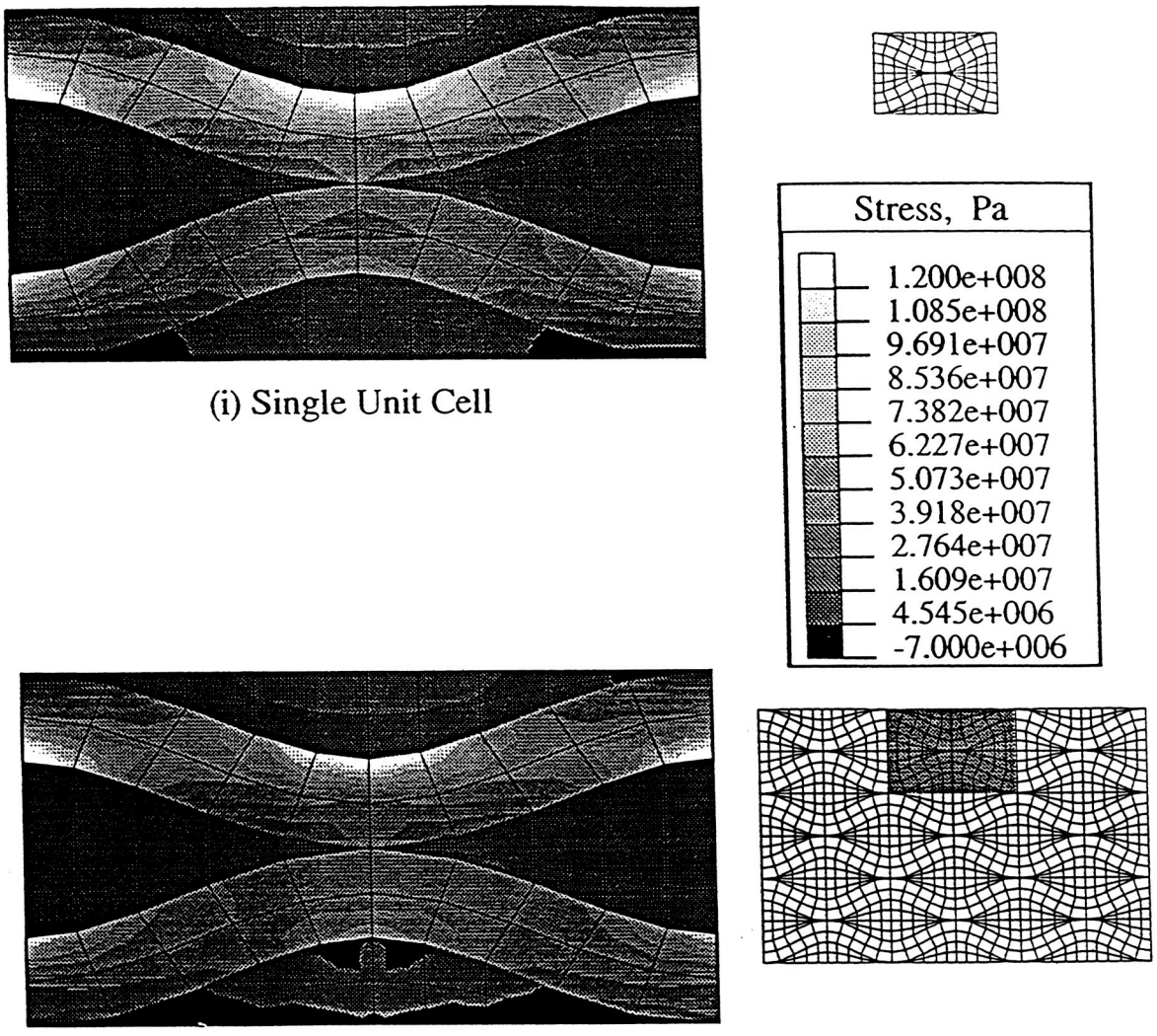

(i) Single Unit Cell

(ii) Exterior Unit Cell of a (3x3) unit cell model

(a) Axial Stress

Figure 9 Stress contours for a two dimensional model of a plain weave composite under bending. (nominal axial strain at top surface = .001)

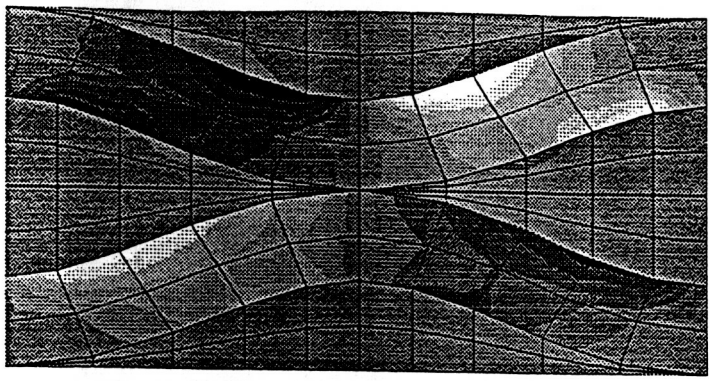

(i) Single Unit Cell

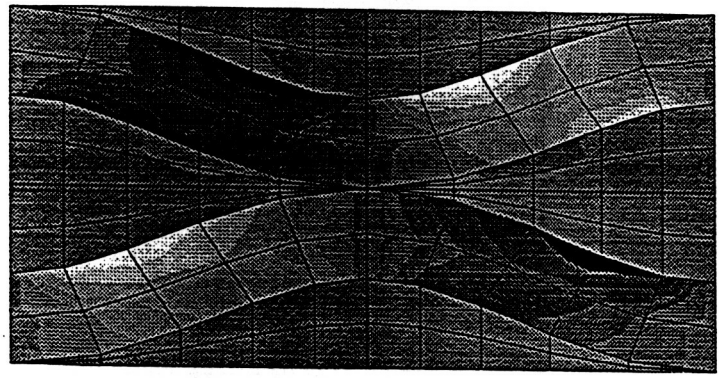

(ii) Exterior Unit Cell of a (3x3) unit cell model

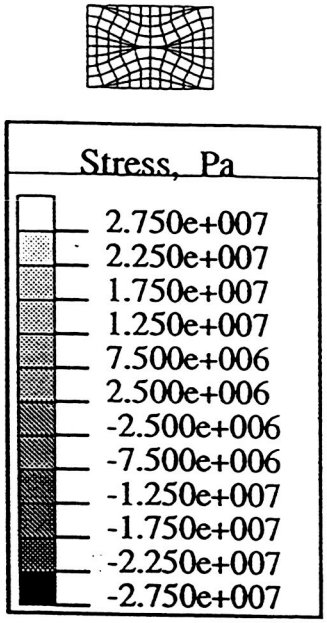

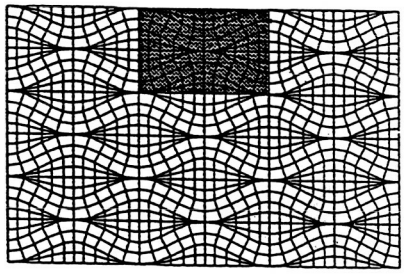

(c) Shear Stress

Figure 9, Concluded.

REPORT DOCUMENTATION PAGE

Form Approved
OMB No. 0704-0188

1. AGENCY USE ONLY (*Leave blank*)	2. REPORT DATE	3. REPORT TYPE AND DATES COVERED
	April 1994	Final Contractor Report

4. TITLE AND SUBTITLE

Analysis of New Composite Architectures

5. FUNDING NUMBERS

WU–505–62–10
G–NAG3–1270

6. AUTHOR(S)

John D. Whitcomb

7. PERFORMING ORGANIZATION NAME(S) AND ADDRESS(ES)

Aerospace Engineering Department
and Center for Mechanics of Composites
Texas A&M University
College Station, Texas 77843–3141

8. PERFORMING ORGANIZATION REPORT NUMBER

E–8705

9. SPONSORING/MONITORING AGENCY NAME(S) AND ADDRESS(ES)

National Aeronautics and Space Administration
Lewis Research Center
Cleveland, Ohio 44135–3191

10. SPONSORING/MONITORING AGENCY REPORT NUMBER

NASA CR–195303

11. SUPPLEMENTARY NOTES

Project Manager, Christos C. Chamis, Structures Division, NASA Lewis Research Center, organization code 5200, (216) 433–3252.

12a. DISTRIBUTION/AVAILABILITY STATEMENT

Unclassified - Unlimited
Subject Category 24

12b. DISTRIBUTION CODE

13. ABSTRACT ***(Maximum 200 words)***

Global/local method in conjunction with a special macro finite element is used to gain computational efficiency in the simulation of textile composites behavior. Results are included to demonstrate the effectiveness of the method. Also, two dimensional finite elements are used to study boundary effects in plain weave composite specimens subjected to extension, shear, and flexure loads. Effective extension, shear, and flexural moduli were found to be quite sensitive to specimen size. For extension and flexure loads stress distributions were affected by a free surface, but the free surface boundary effect did not appear to propagate very far into the interior. For shear load the boundary effect appeared to propagate much further into the interior. The report is in the form of two technical articles, the first describes the global/local method while the second describes the use of the two dimensional finite elements.

14. SUBJECT TERMS

Textiles; Woven composites; Finite elements; Stress analysis; Boundary effects

15. NUMBER OF PAGES
52

16. PRICE CODE
A04

17. SECURITY CLASSIFICATION OF REPORT	18. SECURITY CLASSIFICATION OF THIS PAGE	19. SECURITY CLASSIFICATION OF ABSTRACT	20. LIMITATION OF ABSTRACT
Unclassified	Unclassified	Unclassified	